

A fast method to compute dispersion diagrams of three-dimensional photonic crystals with rectangular geometry

Vadim A. Markel^{a,*}, Markus Schöbinger^b and Karl Hollaus^b

^aDepartment of Radiology, University of Pennsylvania, Philadelphia, Pennsylvania 19104, USA

^bTechnische Universität Wien, Institute for Analysis and Scientific Computing, A-1040 Vienna, Austria

ARTICLE INFO

Keywords:

Photonic crystals
Dispersion
Continued fraction

Published in:

Computer Physics Communications
279, 108441 (2022)
doi: 10.1016/j.cpc.2022.108441

ABSTRACT

We propose a method and codes for fast computation of complex dispersion relations in three-dimensional photonic crystals (PCs) with rectangular geometry. The main idea of the method is to convert the eigenproblem to a nonlinear equation equivalent to the zero-determinant condition. This equation is then solved iteratively either by fixed-point iteration or by rational approximation method. Additional mathematical elements include fast-converging continued-fraction expansion to compute the interaction tensor (appearing in the above nonlinear equation) and efficient accounting for the rectangular geometry in matrix-vector multiplications, which are involved in computing the continued fraction coefficients. The method allows one to perform realistic three-dimensional computations on a typical laptop computer, including finding the Bloch wave vector in the band gaps and in evanescent mode bands. This paper is focused on the method and includes its detailed explanation and illustration with examples. The associated computational package contains a detailed user guide and a set of further demonstrations, which can be run with the help of provided scripts.

Program summary

Program Title: RectDisp v.1-3

CPC Library link to program files: (to be added by Technical Editor)

Code Ocean capsule: (to be added by Technical Editor)

Licensing provisions: CC BY NC 3.0

Programming language: Fortran 2003

Nature of problem: The program computes the complex Bloch wave number \mathbf{q} as a function of real frequency ω in photonic crystals (PCs) with rectangular geometry. The PC constituents are characterized by complex dispersive permittivities and are non-magnetic. Projection of \mathbf{q} onto the XY -plane of the PC is fixed and can be specified by the user, and the projection onto the Z -axis is computed.

Solution method: The method converts the eigenproblem of finding \mathbf{q} to the nonlinear equation equivalent to the zero-determinant condition for, at most, a 3×3 matrix, and solves the latter by an iterative method (either fixed-point iteration or rational approximation or a combination of the two approaches). Additional features include continued-fraction expansion for computing the coefficients in the nonlinear equation and utilization of variable separability characteristic of the rectangular geometry for fast matrix-vector multiplication.


Additional comments including restrictions and unusual features: The current version of the codes compute at most one value of \mathbf{q} for each frequency. This excludes spurious modes arising due to the artificial band folding. Such modes are usually not coupled to incident radiation. However, some other modes can be missed. Under most circumstances, this can happen at higher frequencies, i.e., for $\omega h/c > \pi$, where h is the PC period. Verification of mode coupling to external radiation and exhaustive search for all coupled modes are not currently implemented but we plan to add these features in future releases. If a solution is not found at some frequency, it can potentially be found by fine-tuning input parameters as described in the User Guide.

1. Introduction

Three-dimensional full-wave electromagnetic simulations remain demanding even with modern computers. While many electromagnetic software packages are currently available, most of them are designed to handle objects of rather general geometry and properties. But generality and efficiency do not come easily together, as is well


known in numerical analysis. Therefore, development of specialized methods that provide high performance for a narrow class of problems is still of considerable interest. In this paper, we describe a specialized method and present codes for computing the dispersion relations (more precisely, some restrictions of the Bloch variety) of three-dimensional photonic crystals (PCs) with a rectangular geometry of both the elementary cell and the inclusions. The paper is focused on the theory, detailed explanation of the method and illustrative examples. The associated computational package contains a User Guide with detailed instructions on the code usage, as well as a number of further examples, which can be run directly or with the help of provided scripts.

*Corresponding author

 vmarkel@upenn.edu (V.A. Markel);

markus.schoebinger@tuwien.ac.at (M. Schöbinger);

karl.hollaus@tuwien.ac.at (K. Hollaus)

 <http://whale.seas.upenn.edu/vmarkel> (V.A. Markel)

ORCID(s): 0000-0002-9748-6865 (V.A. Markel); 0000-0003-3429-1419 (M. Schöbinger); 0000-0002-0395-629X (K. Hollaus)

PCs have many applications in science and technology [1]. For instance, sharp features in the transmission and reflection spectra near the edges of photonic band-gaps can be utilized in optical filters and sensors [2–5]. Other PC-based devices include waveguides and interconnects [6], optical diodes [7] and optical elements for collimation and focusing of light [8]. In these and many other applications, precise and efficient computation of dispersion relations is an important part of optical design.

The conventional methods of such computations start from the assumption that the PC constituents are characterized by constant and positive permittivities. Then, by using a Bloch ansatz with a real wave vector \mathbf{q} , one can reduce Maxwell's equations to a Hermitian eigenproblem [9]. The eigenvalue in this formulation is the squared frequency, ω^2 . Eigenvalues of a Hermitian problem are real but can be positive or negative. Therefore, the frequency ω corresponding a selected \mathbf{q} is either real (in the pass bands) or imaginary (in the band gaps). Thus, the conventional methods access one possible *restriction* of the Bloch variety. By Bloch variety we mean here the set of all, generally, complex pairs (ω, \mathbf{q}) for which Maxwell's equations have a nontrivial solution in the PC. A restriction of the Bloch variety is a subset obtained by applying additional constraints.

The conventional restriction obtained by requiring that \mathbf{q} be real and viewing it as a mathematically-independent variable, which is scanned in a computation, has obvious drawbacks. For example, one can determine that a certain real frequency ω_0 is in a gap (that is, there are no real eigenfrequencies ω in the vicinity of ω_0). However, in an experiment, it is possible to illuminate the PC by a quasi-monochromatic light at the real frequency ω_0 . The conventional methods do not provide information about the complex Bloch wave vector at $\omega \approx \omega_0$. Besides, realistic materials are dispersive, have nonzero absorption¹ and can even be metals. Finally, the conventional methods are incapable of describing the evanescent modes, which are characterized by general complex \mathbf{q} . Accounting for the evanescent modes is important, for instance, in problems involving interfaces and tunneling [10, 11] and in PCs containing metallic components [12].

The above limitations have motivated interest in a more physically-relevant restriction of the Bloch variety, often referred to as complex dispersion relations [13–15]. To define this variety, we select the real frequency ω as the mathematically-independent variable and, for each ω considered, compute the complex Bloch wave vector \mathbf{q} . By scanning ω , we can sample the *dispersion relation* $\mathbf{q}(\omega)$ where ω is real but \mathbf{q} can be complex. Note that this approach is more general than just selecting a different restriction of the same variety. Indeed, since ω is now mathematically-independent, it is easy to include into consideration dispersive and therefore complex permittivities of the PC constituents. Thus, not only we select a different restriction, but also can now consider more general Bloch varieties.

¹Small absorption can be accounted for in the conventional methods perturbatively.

The price of above improvements is increased mathematical complexity. Indeed, complex dispersion relations require solution of a quadratic eigenproblem, which can be transformed to a linear problem but without any special symmetry. The matrix in this case is neither symmetric nor Hermitian, and the computational complexity can become prohibitively high, especially in three dimensions. Numerical investigation of complex dispersion relations began in 1990-ies. The problem was initially attacked using the transfer matrix method [16, 17]. The deficiency of this approach is that it requires determination of the eigenvalues of a matrix with an exponentially large condition number. In practice, this cannot be done without an almost absolute loss of precision [18]. There are other issues associated with the transfer matrix method and it is rarely used at present. Plane-wave expansion of the fields and algebraic solution of the quadratic eigenproblem by direct methods such as those implemented in EISPACK was another popular approach [10, 12, 19]. The condition number in this case is not exponentially large but the computational complexity of direct methods scales as L^9 in three dimensions, where L is the number of discretization units (either plane waves or real-space points) in one spatial direction. This has, essentially, limited the applicability of the method to two dimensions. Yet another approach utilized finite difference time domain (FDTD) discretization to extract complex modes from the transmission coefficient of a finite structure [20]. The methods requires introduction of perfectly-matched layers in order to achieve a finite computational domain and is similar in spirit to the transfer matrix method. More recent approaches to computing complex dispersion relations in three-dimensional PCs are mostly focused on constructing special bases for discretization and then solving the ensuing eigenproblem by Krylov-subspace methods such as Arnoldi iteration [13, 15, 21]. Recently, a stochastic approach to solving the eigenproblem was also proposed [22].

In this paper, we utilize the plane wave basis for discretization but then take a somewhat unorthodox approach and compute the eigenvalues of interest by considering the nonlinear equation, which is equivalent to the zero-determinant condition for the original matrix. However, we use the fundamental theorem of determinants of block matrices to state this condition for a matrix of the size 3×3 at most. We then solve the ensuing nonlinear equation iteratively. Of course, it is common knowledge that reducing an eigenproblem to the zero-determinant condition is not an efficient way to compute the eigenvalues. In fact, the reverse order of steps is preferred. For example, a stable way to find the roots of a high-order polynomial is to construct the companion matrix and then compute its eigenvalues by the methods of matrix algebra. However, we will show that, for the Bloch variety problem, one can safely use the zero-determinant condition.

The situation is somewhat similar to solving the equation $z = e^{-z}$, which can be approximated by a polynomial in a circle of a finite radius R . The equation has infinitely many

roots in the complex plane, but only one real root². The latter can be easily found by a simple fixed-point iteration. If this root is all one needs, there is no reason to consider the more complicated equation. Otherwise, one can expand the exponent to some finite but sufficient order, reduce the equation to a polynomial, and construct the companion matrix. The roots of the polynomial can be obtained by diagonalizing the latter. Thus we can compute the roots of the equation $z = e^{-z}$ in a circle of an arbitrary radius R by reducing a nonlinear equation to an eigenproblem. In this paper, we adopt a strategy that is in some sense reverse-order; we start from an eigenproblem and reduce it to a nonlinear equation; we then solve this equation iteratively guided by the knowledge that we need only one or two physically-relevant roots. One simplification that will ensue is that we will not need to store or manipulate any large matrices; the memory requirements of the proposed method are modest, which is unusual for three-dimensional problems.

There are two other important mathematical elements that we will employ. First, we will use rapidly-converging continued-fraction expansions to arrive at the nonlinear equation mentioned above. In fact, the method proposed here is also in some sense a Krylov-subspace method; we just use the Krylov basis to arrive at the nonlinear equation rather than to search for the eigenvalues directly. This is advantageous since, as we will show, the algebraic computations will be reduced to solving a system of equations but not for all the unknowns; rather, we will need projections of the solution onto at most three basis vectors. Such computations can be efficient with the use of continued fraction expansions. Second, we will specialize to rectangular geometry of both the lattice and the inclusions. In this case, one can exploit separation of variables to compute the coefficients in the continued fraction. If we use L basis functions in one spatial dimensions, the overall computational complexity of the algorithm scales as ML^4 where M is the number of iterations. For comparison, direct methods for solving the dispersion relations in three-dimensional PCs by diagonalization scale as L^9 and general iterative methods scale as ML^6 . Two-dimensional and one-dimensional problems can be considered as special cases, which the codes can handle easily. The computational complexity scales as ML^3 for two-dimensional problems and as ML^2 for one-dimensional problems. Of course, we should keep in mind that any one-dimensional PC with just two layers can be solved analytically; the capability to solve one-dimensional problems in the codes is included only for making comparisons.

We will use Fourier (plane wave) basis and thus avoid the technical complexities of the finite difference or finite element methods. This basis is commensurate with the rectangular geometry. The nonlinear equation expressing the zero-determinant condition will be solved by the fixed-point iteration or the rational approximation methods or a combination of these methods. With the mathematical developments briefly described above, this results in a rather simple

algorithm, which is easy to program and which can perform realistic three-dimensional electromagnetic computations on a simple laptop computer on the timescale of seconds or minutes. Of course, as any computational method, the method proposed here can be broken or become slow, but the set of examples provided with the codes will illustrate the relevant range of applicability. These examples can be changed and generalized by the users.

The rest of this paper is organized as follows. In Section 2 we introduce the problem geometry and basic notations. In Section 3 we reduce the dispersion equation in a PC to a nonlinear equation expressing the condition that the determinant of the characteristic matrix is zero. This derivation is based on our previous work [23–25], and here we also prove the main result using the theory of determinants of block matrices. Also, in this section we introduce the *interaction tensor* – the key mathematical ingredient of the proposed method. The zero-determinant condition depends on this tensor, and its algebraic computation is the most intensive part of the proposed algorithm. In Section 4, we show how the interaction tensor can be computed efficiently. The specific properties of the rectangular geometry are used at this stage. Also in this section we analyze the computational complexity of the proposed algorithm. In Section 5, we discuss the Bloch wave polarization modes, which appear by considering the zero-determinant condition, and the ensuing nonlinear equation. Section 6 contains a detailed numerical illustration of the method and a few examples of dispersion calculations including more difficult cases. In Section 7, we provide validation of the proposed methods by direct comparison with computations based on finite-element discretization of the field and Arnoldi iterations for the resulting polynomial eigenproblem. In Section 8, we give a brief self-consistent summary of the proposed method. Finally, Section 9 contains a discussion.

2. Problem geometry and set up

Consider a PC with a general orthorhombic lattice. The unit cell is a parallelepiped with the sides h_x , h_y and h_z (we work in a reference frame whose axes XYZ coincide with the crystallographic axes of the PC). Further, each unit cell contains a parallelepiped-shaped inclusion with the sides $2a_x$, $2a_y$ and $2a_z$. Without loss of generality, we can assume that both parallelepipeds (the unit cell and the inclusion) have a common center. Note that geometrical consistency requires that $a_\alpha \leq h_\alpha/2$. Here and below small Greek indexes α, β, γ take the values of x, y or z . For later convenience, we denote by a_α *one half* of the inclusion side length. In what follows, we refer to PCs of this type as simply *rectangular*.

The inclusions and the host medium are characterized by the dielectric permittivities $\epsilon_i(\omega)$ and $\epsilon_h(\omega)$, respectively, where ω is the electromagnetic frequency. The host and inclusions are assumed to be intrinsically non-magnetic. Generalization to magnetic media is in principle possible but not of interest at high frequencies. Thus, the PC is fully characterized by its position- and frequency-dependent

²One can reduce the complex equation $z = e^{-z}$ to the real equation $x + \exp(x \operatorname{ctg}(x)) \sin(x) = 0$.

permittivity $\epsilon(\mathbf{r}, \omega)$. Using the above assumptions, we can write

$$\epsilon(\mathbf{r}, \omega) = \epsilon_h(\omega) + [\epsilon_i(\omega) - \epsilon_h(\omega)]\Theta(\mathbf{r}), \quad (1)$$

where $\Theta(\mathbf{r})$ is the shape function: it is equal to unity inside an inclusion and to zero in the host. In what follows, the dependence of ϵ_i , ϵ_h and ϵ on the electromagnetic frequency is implied but not included explicitly in the list of formal arguments. That is, we write $\epsilon(\mathbf{r})$ instead of $\epsilon(\mathbf{r}, \omega)$, etc. From the discrete periodicity of the PC, it follows that $\epsilon(\mathbf{r})$ can be expanded as

$$\epsilon(\mathbf{r}) = \sum_{\mathbf{g}} \epsilon_{\mathbf{g}} e^{i\mathbf{g}\cdot\mathbf{r}}, \quad (2)$$

were

$$\mathbf{g} = \left(\frac{2\pi n_x}{h_x}, \frac{2\pi n_y}{h_y}, \frac{2\pi n_z}{h_z} \right) \quad (3)$$

are the reciprocal lattice vectors (RLVs) and n_x , n_y and n_z are arbitrary integers. Note that we use the notation involving summation over \mathbf{g} (as in (2)) as a shorthand for summation over the triplet of associated integers.

The expansion coefficients in (2) can be written in the form

$$\epsilon_{\mathbf{g}} = \epsilon_h [\delta_{\mathbf{g}\mathbf{0}} + \chi M(\mathbf{g})], \quad (4)$$

where $\delta_{\mathbf{g}\mathbf{p}}$ is the Kronecker delta-symbol acting on the RLVs (or triplets of associated integers), $\mathbf{0}$ is the trivial RLV corresponding to $(n_x, n_y, n_z) = (0, 0, 0)$,

$$\chi = \rho \frac{\epsilon_i - \epsilon_h}{\epsilon_h} \quad (5)$$

is a scalar parameter, which quantifies the degree of inhomogeneity of the PC,

$$\rho = \frac{V_i}{V_C} = \frac{8a_x a_y a_z}{h_x h_y h_z} \quad (6)$$

is the volume fraction of inclusions (V_i is the volume of one inclusion, V_C is the volume of one unit cell), and

$$M(\mathbf{g}) = \frac{1}{V_i} \int_{\mathcal{C}} \Theta(\mathbf{r}) e^{-i\mathbf{g}\cdot\mathbf{r}} d^3r. \quad (7)$$

The integration in this formula is over one unit cell and the function $\Theta(\mathbf{r})$ further restricts the integration region to the inclusion. The function $M(\mathbf{g})$ has been defined so that $M(\mathbf{0}) = 1$ and $\sum_{\mathbf{g}} M(\mathbf{g}) = 1/\rho$. For the latter equality to hold, the center of the unit cell must be inside the inclusion, as we assume here; otherwise, the sum is zero.

Below, we will rely on the following important observation: in a rectangular PC, $M(\mathbf{g})$ are separable, that is, if $\mathbf{g} = (g_x, g_y, g_z)$, then

$$M(\mathbf{g}) = M_x(g_x)M_y(g_y)M_z(g_z), \quad (8a)$$

where

$$M_{\alpha}(g_{\alpha}) = \frac{\sin(g_{\alpha}a_{\alpha})}{g_{\alpha}a_{\alpha}} = \frac{\sin(2\pi n_{\alpha}a_{\alpha}/h_{\alpha})}{2\pi n_{\alpha}a_{\alpha}/h_{\alpha}}. \quad (8b)$$

Here we have also used the expression (3) for RLVs in terms of triplets of integers (n_x, n_y, n_z) .

Note that the expressions (4), (7) have been introduced in [23–25] in a more general setting. However, the expressions (6) and, more importantly, (8) are specific to rectangular PCs. Finally, $M(\mathbf{u})$ is defined mathematically for a generic vector argument \mathbf{u} . However, this function is used below in a such a way that its argument is either a RLV or a difference between two RLVs, as in $M(\mathbf{g} - \mathbf{p})$. Note that, for Bravais lattices, a sum of two RLVs is also a RLV.

3. Dispersion equation in a rectangular PC

The starting point for the derivations of this paper is the frequency-domain Maxwell's equation for the electric field, written in the form

$$\nabla \times \nabla \times \mathbf{E}(\mathbf{r}) = k^2 \epsilon(\mathbf{r}) \mathbf{E}(\mathbf{r}), \quad k = \omega/c. \quad (9)$$

Here k is the free-space wave number at the frequency ω . We work in the frequency domain and write all fields that are functions of position and time in the form $\text{Re}[\mathbf{E}(\mathbf{r})e^{-i\omega t}]$.

The solution to (9) with $\epsilon(\mathbf{r})$ defined in (1)-(7) can be sought using the ansatz

$$\mathbf{E}(\mathbf{r}) = \sum_{\mathbf{g}} \mathbf{E}_{\mathbf{g}} e^{i(\mathbf{q}+\mathbf{g})\cdot\mathbf{r}}, \quad (10)$$

where the wave vector \mathbf{q} and the constant coefficients $\mathbf{E}_{\mathbf{g}}$ must be determined. Importantly, (10) is a solution to (9) only for some special values of \mathbf{q} . We say that, if (10) with some $\mathbf{q} = \mathbf{q}_B$ satisfies (9), then \mathbf{q}_B is the Bloch wave vector. Computing numerically the *dispersion function* $\mathbf{q}_B(\omega)$ is the main goal of this paper. In this computation, ω is assumed to be real-valued but the components of \mathbf{q}_B can be complex. We therefore expect that $\mathbf{q}_B(\omega)$ is defined (but can be multi-valued) for all positive ω .

By substituting (10) and (2) into (9) and accounting for orthogonality of the functions $e^{i\mathbf{g}\cdot\mathbf{r}}$ over a unit cell, we arrive at the equation

$$(\mathbf{q} + \mathbf{g}) \times (\mathbf{q} + \mathbf{g}) \times \mathbf{E}_{\mathbf{g}} + k^2 \sum_{\mathbf{p}} \epsilon_{\mathbf{g}-\mathbf{p}} \mathbf{E}_{\mathbf{p}} = 0. \quad (11)$$

We then use the expression (4) for $\epsilon_{\mathbf{g}-\mathbf{p}}$ to re-write (11) as

$$(\mathbf{q} + \mathbf{g}) \times (\mathbf{q} + \mathbf{g}) \times \mathbf{E}_{\mathbf{g}} + k^2 \left[\epsilon_h \mathbf{E}_{\mathbf{g}} + \epsilon_h \chi \sum_{\mathbf{p}} M(\mathbf{g} - \mathbf{p}) \mathbf{E}_{\mathbf{p}} \right] = 0. \quad (12)$$

Following Refs. [23–25], we treat the cases $\mathbf{g} = \mathbf{0}$ and $\mathbf{g} \neq \mathbf{0}$ separately. Thus, by setting $\mathbf{g} = \mathbf{0}$ in (12), we obtain

$$\mathbf{q} \times \mathbf{q} \times \mathbf{E}_{\mathbf{0}} + k^2 \left[\langle \epsilon \rangle \mathbf{E}_{\mathbf{0}} + \epsilon_h \chi \sum_{\mathbf{g} \neq \mathbf{0}} M(-\mathbf{g}) \mathbf{E}_{\mathbf{g}} \right] = 0, \quad (13)$$

where

$$\langle \epsilon \rangle = \epsilon_0 = \rho \epsilon_i + (1 - \rho) \epsilon_h \quad (14)$$

is the average permittivity of the PC. Note that summation in (13) does not contain \mathbf{E}_0 .

The following observation is crucial for the derivation presented here. Namely, from the linearity of (12), it follows that there exists a 3×3 matrix $\Sigma(\mathbf{q})$ such that

$$\sum_{\mathbf{g} \neq \mathbf{0}} M(-\mathbf{g}) \mathbf{E}_{\mathbf{g}} = \Sigma(\mathbf{q}) \mathbf{E}_0. \quad (15)$$

We refer to $\Sigma(\mathbf{q})$ as to the *interaction tensor*. It is uniquely defined by the PC geometry, the electromagnetic frequency ω and the vector \mathbf{q} . In the notation $\Sigma(\mathbf{q})$, we include only \mathbf{q} in the list of formal arguments since this dependence on \mathbf{q} will be exploited below to compute $\mathbf{q}_B(\omega)$. A practical method for computing $\Sigma(\mathbf{q})$ is given in Section 4.

We can now re-write (13) as

$$[(\mathbf{q} \times \mathbf{q} \times) + k^2 \langle \epsilon \rangle + k^2 \epsilon_h \chi \Sigma(\mathbf{q})] \mathbf{E}_0 = 0. \quad (16)$$

The above equation has a non-trivial solution for \mathbf{E}_0 if and only if the determinant of the 3×3 matrix in the square brackets is zero. Denoting this matrix by $\Pi(\mathbf{q})$, we arrive at the following condition for \mathbf{q} to be a Bloch wave vector:

$$\det[\Pi(\mathbf{q})] = 0, \quad (17)$$

where

$$\Pi_{\alpha\beta}(\mathbf{q}) = q_\alpha q_\beta + (k^2 \langle \epsilon \rangle - q^2) \delta_{\alpha\beta} + k^2 \epsilon_h \chi \Sigma_{\alpha\beta}(\mathbf{q}). \quad (18)$$

Here $q^2 = q_x^2 + q_y^2 + q_z^2$ and we have used the triple vector product formula $\mathbf{q} \times \mathbf{q} \times \mathbf{E}_0 = \mathbf{q}(\mathbf{q} \cdot \mathbf{E}_0) - q^2 \mathbf{E}_0$. Assuming that the interaction tensor $\Sigma(\mathbf{q})$ is known or can be computed, we will seek $\mathbf{q}_B(\omega)$ by solving the nonlinear equation (17) at various values of ω .

It should be noted that $\Sigma(\mathbf{q})$ and $\Pi(\mathbf{q})$ are defined for all \mathbf{q} but are not lattice-periodic. However, if some \mathbf{q}^* is a root of (17), then $\mathbf{q}^* + \mathbf{g}$ is also a root, where \mathbf{g} is an arbitrary RLV. This statement is true assuming $\Sigma(\mathbf{q})$ was computed using the whole infinite set of RLVs. For any finite truncation, the property is approximate and tends to lose precision for large \mathbf{g} 's. Numerical methods developed in this paper take this into account as described in Section 6.

Derivation of (17) from (16) is straightforward. However, derivation (16) from (12) may not be as obvious or familiar. To the best of authors' knowledge, Eq. (16) is not widely known or understood. Considering the fundamental importance of (16) in the physics of PCs, we provide below an alternative derivation based on the theory of determinants of block matrices [26, 27]. Consider a square block matrix X of the form

$$X = \begin{bmatrix} A & B \\ C & D \end{bmatrix}, \quad (19)$$

where A , B , C and D are blocks of arbitrary size (B and C may not be square) with the only constraint that they fill X

completely and have one common vertex. The basic theorem in this field states that the determinant of X is given by

$$\det[X] = \det[A - BD^{-1}C] \det[D]. \quad (20)$$

In the case when A , B , C , and D are numbers, this expression becomes the well-known formula for a 2×2 matrix. In a more general setting, (20) is not as trivial but can be proved using multiplicativity of determinants. For our purposes, the following fact is important: if D is invertible, then the conditions $\det[X] = 0$ and $\det[A - BD^{-1}C] = 0$ are equivalent.

Now, (12) is an infinite set of homogeneous linear equations, which can be written formally as $Xe = 0$ where e is a vector with the elements $(\mathbf{E}_{\mathbf{g}})_\alpha$, and

$$X_{\mathbf{g}\alpha, \mathbf{p}\beta} = [(\mathbf{q} + \mathbf{g})_\alpha (\mathbf{q} + \mathbf{g})_\beta + (k^2 \epsilon_h - (\mathbf{q} + \mathbf{g})^2) \delta_{\alpha\beta}] \delta_{\mathbf{g}\mathbf{p}} + k^2 \epsilon_h \chi M(\mathbf{g} - \mathbf{p}) \delta_{\alpha\beta}. \quad (21)$$

The condition for $Xe = 0$ to have a non-trivial solution is $\det[X] = 0$, and we wish to apply theorem (20) to $\det[X]$. To this end, we partition X into four blocks. Let us arrange the matrix elements with $\mathbf{g} = \mathbf{p} = \mathbf{0}$ in the top-left corner of X . In this case, X is infinitely continued down and to the right. We then define the 3×3 top-left corner block A with the elements

$$A_{\alpha\beta} = q_\alpha q_\beta + (k^2 \langle \epsilon \rangle - q^2) \delta_{\alpha\beta}. \quad (22)$$

The semi-infinite block B of the size $3 \times \infty$ is directly to the right of A ; its elements correspond to $\mathbf{g} = \mathbf{0}$, $\mathbf{p} \neq \mathbf{0}$ and are of the form:

$$B_{\alpha, \mathbf{p}\beta} = k^2 \epsilon_h \chi M(-\mathbf{p}) \delta_{\alpha\beta}, \quad \mathbf{p} \neq \mathbf{0}. \quad (23)$$

Similarly, the block C directly below A contains the elements with $\mathbf{g} \neq \mathbf{0}$, $\mathbf{p} = \mathbf{0}$. The elements of C are

$$C_{\mathbf{g}\alpha, \beta} = k^2 \epsilon_h \chi M(\mathbf{g}) \delta_{\alpha\beta}, \quad \mathbf{g} \neq \mathbf{0}. \quad (24)$$

Finally, the block D is below B and to the right of C ; it touches A at the top-left corner. The elements of D are of the same generic form as in (21), except that we restrict this expression to $\mathbf{g} \neq \mathbf{0}$ and $\mathbf{p} \neq \mathbf{0}$.

Now assume that D is invertible and define $Y = A - BD^{-1}C$. It follows from (20) that the conditions $\det[X] = 0$ and $\det[Y] = 0$ are equivalent. According to the definition, Y is a 3×3 matrix with the elements

$$Y_{\alpha\beta} = q_\alpha q_\beta + (k^2 \langle \epsilon \rangle - q^2) \delta_{\alpha\beta} - (k^2 \epsilon_h \chi)^2 \sum_{\mathbf{g}, \mathbf{p} \neq \mathbf{0}} M(-\mathbf{g}) D_{\mathbf{g}\alpha, \mathbf{p}\beta}^{-1} M(\mathbf{p}). \quad (25)$$

Comparing this expression to (18), we see that $\Pi = Y$ if we identify

$$\Sigma_{\alpha\beta} = -k^2 \epsilon_h \chi \sum_{\mathbf{g}, \mathbf{p} \neq \mathbf{0}} M(-\mathbf{g}) D_{\mathbf{g}\alpha, \mathbf{p}\beta}^{-1} M(\mathbf{p}). \quad (26)$$

This is indeed the algebraic definition of Σ . It can be easily verified that the matrix defined in (26) satisfies (15). We

note that, in order to compute Σ , the whole inverse matrix D^{-1} is not needed; we only need several matrix elements. Considering that Σ is symmetric³, we need at most 6 matrix elements. In Section 4, we explain how these matrix elements can be computed without inverting the matrix D directly or solving large sets of linear equations.

It remains to discuss what would happen if D was not invertible. Although we do not have a mathematical proof, we never encountered singular D 's in simulations. In fact, singularity of D is unphysical; it would result in one of two possibilities: either solutions to Maxwell's equation (9) do not exist in the PC at all, or such solutions are non-unique under the conditions when we can expect uniqueness on physical grounds. Perhaps, D can become singular in amplifying media with $\text{Im}\epsilon < 0$ wherein stationary harmonic solutions do not satisfy time-domain Maxwell's equations. But we do not consider such cases in this paper. Therefore, in what follows, we assume that D or its finite truncations are invertible.

4. Computing the interaction tensor

In principle, the interaction tensor is defined by (26). However, in most cases of interest, the matrix D is large and its direct inversion is neither possible nor really needed. In fact, working with D numerically is not the best approach, and we will introduce an analytical transformation of (26), which can be used to devise an efficient numerical method for computing Σ .

We already considered the case $\mathbf{g} = \mathbf{0}$ in Eqs. (13), (16). Now let us write (12) for $\mathbf{g} \neq \mathbf{0}$. With some re-arrangement and using the triple vector product formula, we obtain

$$\begin{aligned} & [(\mathbf{q} + \mathbf{g})^2 - k^2\epsilon_h] \mathbf{E}_{\mathbf{g}} - (\mathbf{q} + \mathbf{g}) ((\mathbf{q} + \mathbf{g}) \cdot \mathbf{E}_{\mathbf{g}}) = \\ & = k^2\epsilon_h\chi \left[M(\mathbf{g})\mathbf{E}_0 + \sum_{\mathbf{p} \neq \mathbf{0}} M(\mathbf{g} - \mathbf{p})\mathbf{E}_{\mathbf{p}} \right], \quad \mathbf{g} \neq \mathbf{0}. \end{aligned} \quad (27)$$

In the right-hand side of the above equation, we have split the summation over \mathbf{p} into the $\mathbf{p} = \mathbf{0}$ and $\mathbf{p} \neq \mathbf{0}$ terms. We now notice that the matrix in the left-hand side of (27) is invertible. Indeed, consider the linear equation for a generic vector \mathbf{u} :

$$(s^2 - w)\mathbf{u} - \mathbf{s}(\mathbf{s} \cdot \mathbf{u}) = \mathbf{b}, \quad (28)$$

where $s^2 = \mathbf{s} \cdot \mathbf{s}$. Assuming $w \neq 0$ and $w \neq s^2$, the solution to (28) is

$$\mathbf{u} = \frac{1}{w} \frac{w\mathbf{b} - \mathbf{s}(\mathbf{s} \cdot \mathbf{b})}{s^2 - w}. \quad (29)$$

Using this result, we can transform (27) identically as

$$\mathbf{E}_{\mathbf{g}} = \chi K(\mathbf{q} + \mathbf{g}) \left[M(\mathbf{g})\mathbf{E}_0 + \sum_{\mathbf{p} \neq \mathbf{0}} M(\mathbf{g} - \mathbf{p})\mathbf{E}_{\mathbf{p}} \right], \quad (30)$$

³ Since D is symmetric and the set of RLVs over which the summation in (26) runs can be partitioned completely into pairs of the form $\{\mathbf{g}, -\mathbf{g}\}$.

where

$$K_{\alpha\beta}(\mathbf{u}) = \frac{k^2\epsilon_h\delta_{\alpha\beta} - u_\alpha u_\beta}{u^2 - k^2\epsilon_h}. \quad (31)$$

Here \mathbf{u} is a generic three-dimensional vector and $K(\mathbf{u})$ is a 3×3 matrix.

The form of Eq. (30) is convenient in several respects. For example, it can be iterated to obtain an expansion of $\Sigma(\mathbf{q})$ in powers of χ . The first non-vanishing term in this expansion is

$$\Sigma^{(1)}(\mathbf{q}) = \chi \sum_{\mathbf{g} \neq \mathbf{0}} M(-\mathbf{g})K(\mathbf{q} + \mathbf{g})M(\mathbf{g}), \quad (32a)$$

or, in components,

$$\Sigma_{\alpha\beta}^{(1)}(\mathbf{q}) = \chi \sum_{\mathbf{g} \neq \mathbf{0}} M(-\mathbf{g}) \frac{k^2\epsilon_h\delta_{\alpha\beta} - (\mathbf{q} + \mathbf{g})_\alpha(\mathbf{q} + \mathbf{g})_\beta}{(\mathbf{q} + \mathbf{g})^2 - k^2\epsilon_h} M(\mathbf{g}). \quad (32b)$$

We have already noticed that Σ is symmetric (see footnote 3). This property is general for orthorhombic lattices and independent of the inclusion shape. Additional symmetry properties that are specific to rectangular inclusions can be inferred from (32b). Note that these properties hold beyond first-order approximation and therefore are exact. Thus, if \mathbf{q} has only one Cartesian component (in a frame coinciding with the crystallographic axes), then Σ is diagonal. If, in addition, the inclusion is cubic, all diagonal elements of Σ are equal. If \mathbf{q} lies in one of the crystallographic planes, say, XY , then Σ has one nonzero off-diagonal element Σ_{xy} but $\Sigma_{xz} = \Sigma_{yz} = 0$. If \mathbf{q} has non-zero projections onto all three axes, then Σ is a full matrix with 6 independent elements.

In principle, we can iterate (30) to obtain an expansion of Σ in powers of χ to arbitrary order. Here we consider a different approach, which is applicable, in particular, in the strong interaction regime when χ is not small. By comparing the definition of Σ (15) to (30), we see that

$$\Sigma_{\alpha\beta}(\mathbf{q}) = \langle \mathbf{a}^{(\alpha)} | (\varkappa\mathbf{I} - W(\mathbf{q}))^{-1} | \mathbf{b}^{(\beta)}(\mathbf{q}) \rangle, \quad (33)$$

where $\varkappa = 1/\chi$ is the spectral parameter of the theory, we have used Dirac notations to shorten the expression⁴, \mathbf{I} is the identity matrix, $\mathbf{a}^{(\gamma)}$, $\mathbf{b}^{(\gamma)}(\mathbf{q})$ are vectors and $W(\mathbf{q})$ is a matrix defined by the following relations:

$$\langle \mathbf{g}\alpha | \mathbf{a}^{(\gamma)} \rangle = M(\mathbf{g})\delta_{\alpha\gamma}, \quad (34a)$$

$$\langle \mathbf{g}\alpha | \mathbf{b}^{(\gamma)}(\mathbf{q}) \rangle = K_{\alpha\gamma}(\mathbf{q} + \mathbf{g})M(\mathbf{g}), \quad (34b)$$

$$\langle \mathbf{g}\alpha | W(\mathbf{q}) | \mathbf{p}\beta \rangle = K_{\alpha\beta}(\mathbf{q} + \mathbf{g})M(\mathbf{g} - \mathbf{p}). \quad (34c)$$

In these equations, $\mathbf{g}, \mathbf{p} \neq \mathbf{0}$ and $|\mathbf{b}^{(\gamma)}(\mathbf{q})\rangle$, $W(\mathbf{q})$ depend on \mathbf{q} . The superscripts in $|\mathbf{a}^{(\gamma)}\rangle$, $|\mathbf{b}^{(\gamma)}(\mathbf{q})\rangle$ label different vectors rather than components of a vector. Still, the three indexes

⁴The usual convention regarding Hermitian conjugation applies. For example, it follows from (34a) that $\langle \mathbf{a}^{(\gamma)} | \mathbf{g}\alpha \rangle = M^*(\mathbf{g})\delta_{\alpha\gamma} = M(-\mathbf{g})\delta_{\alpha\gamma}$. However, in the rectangular geometry of this paper, $M^*(\mathbf{g}) = M(\mathbf{g})$ and $M(-\mathbf{g}) = M(\mathbf{g})$.

α, β, γ take the values from the set $\{x, y, z\}$. For example, $\langle \mathbf{g}\alpha | \mathbf{a}^{(x)} \rangle = M(\mathbf{g})\delta_{\alpha x}$, etc. Also note that the first-order approximation (32) can be obtained as $\chi \langle \mathbf{a}^{(\alpha)} | \mathbf{b}^{(\beta)}(\mathbf{q}) \rangle$.

Thus, in order to compute all six independent elements of Σ , one needs six matrix elements of the form (33). For example, we can compute the matrix elements between $|\mathbf{b}^{(x)}\rangle$ and three vectors $|\mathbf{a}^{(x)}\rangle$, $|\mathbf{a}^{(y)}\rangle$ and $|\mathbf{a}^{(z)}\rangle$, between $|\mathbf{b}^{(y)}\rangle$ and two vectors $|\mathbf{a}^{(y)}\rangle$ and $|\mathbf{a}^{(z)}\rangle$, and finally between $|\mathbf{b}^{(z)}\rangle$ and $|\mathbf{a}^{(z)}\rangle$. We can use the following identity [23] to compute the matrix elements in (33) non-perturbatively:

$$\langle \mathbf{a} | (\varkappa \mathbf{I} - \mathbb{W})^{-1} | \mathbf{b} \rangle = \frac{1}{\varkappa} \frac{\langle \mathbf{a} | \mathbf{b} \rangle}{1 - \frac{\langle \mathbf{a} | (\varkappa \mathbf{I} - \mathbb{W})^{-1} \mathbb{W} | \mathbf{b} \rangle}{\langle \mathbf{a} | \mathbf{b} \rangle}}, \quad (35)$$

where

$$\mathbb{P} = \mathbf{I} - \frac{|\mathbf{b}\rangle\langle \mathbf{a}|}{\langle \mathbf{a} | \mathbf{b} \rangle}. \quad (36)$$

The above relation holds for arbitrary \mathbb{W} as long as $\varkappa \neq 0$ and $\varkappa \mathbf{I} - \mathbb{W}$ is non-singular. In particular, (35) holds for non-Hermitian \mathbb{W} and/or complex \varkappa . One caveat is that, as $\langle \mathbf{a} | \mathbf{b} \rangle$ approaches zero, the expression (35) contains a 0/0-type removable singularity. A convenient approach to handle the singularity numerically is to use the identity

$$(\mathbf{I} - \chi \mathbb{W})^{-1} = \mathbf{I} + \chi(\mathbf{I} - \chi \mathbb{W})^{-1} \mathbb{W}. \quad (37)$$

It then follows that, if $\langle \mathbf{a} | \mathbf{b} \rangle = 0$, we have

$$\langle \mathbf{a} | (\mathbf{I} - \chi \mathbb{W})^{-1} | \mathbf{b} \rangle = \chi \langle \mathbf{a} | (\mathbf{I} - \chi \mathbb{W})^{-1} \mathbb{W} | \mathbf{b} \rangle. \quad (38)$$

Then theorem (35) can be applied to (38) with $|\mathbf{b}'\rangle = \mathbb{W}|\mathbf{b}\rangle$ in place of $|\mathbf{b}\rangle$. The ‘‘shifted inverse’’ identity (37) can be used to regularize the recursion introduced below but it was not used in the numerical simulations of this paper as there was not need for this.

Now, we can apply (35) recursively to itself. This results in the following continued-fraction expansion:

$$\langle \mathbf{a} | (\varkappa \mathbf{I} - \mathbb{W})^{-1} | \mathbf{b} \rangle = \frac{\chi \mu_0}{1 - \frac{\chi \mu_1}{1 - \frac{\chi \mu_2}{1 - \dots}}}, \quad \chi = \frac{1}{\varkappa}. \quad (39)$$

The coefficients μ_n in this expansion are determined as follows. Starting from $\mu_0 = \langle \mathbf{a} | \mathbf{b} \rangle$, $|\mathbf{b}_{-1}\rangle = 0$ and $|\mathbf{b}_0\rangle = |\mathbf{b}\rangle$, we compute for $n = 0, 1, \dots$

$$|\mathbf{b}_{n+1}\rangle = \mathbb{W} \left(|\mathbf{b}_n\rangle - \mu_n |\mathbf{b}_{n-1}\rangle \right), \quad \mu_{n+1} = \frac{\langle \mathbf{a} | \mathbf{b}_{n+1} \rangle}{\langle \mathbf{a} | \mathbf{b}_n \rangle}. \quad (40)$$

Depending on the required precision, this expansion must be computed until the coefficients μ_n become sufficiently small as will be illustrated in Sec. 6.

Thus, (39) together with recursion (40) can be used to compute an arbitrary matrix element of the inverse of $\varkappa \mathbf{I} - \mathbb{W}$. By computing the matrix elements between $|\mathbf{a}^{(\alpha)}\rangle$ and $|\mathbf{b}^{(\beta)}\rangle$ defined in (34a),(34b), we find the elements $\Sigma_{\alpha\beta}$ according to (33). The most computationally-intensive operation in

this algorithm is the matrix-vector multiplication in the first equation of (40). However, the separability of $M(\mathbf{g})$, which is expressed mathematically by Eq. 8, allows one to speed-up this operation significantly. This observation is key to the proposed computational method. In the remainder of this section, we provide a quantitative estimate of the computational complexity of matrix-vector multiplication and of the speed-up associated with the separability of $M(\mathbf{g})$.

The matrix \mathbb{W} is infinite and in a practical computation it must be truncated, i.e., by restricting the RLVs to a finite rectangular box. Let us restrict the integers n_α that enter the definition of \mathbf{g} (3) as $-L \leq n_\alpha \leq L$. Then the number of RLVs included in the analysis (i.e., the number of *plane waves*) is $(2L+1)^3 - 1$. Here unity is subtracted because the trivial RLV $\mathbf{g} = \mathbf{0}$ is excluded. We assume that $L \gg 1$ and therefore the number of RLVs in the computational box is $\approx 8L^3$. Further, for each \mathbf{g} , there are three Cartesian components to consider as labeled by α . Therefore, the length of $|\mathbf{a}\rangle$ and $|\mathbf{b}\rangle$ is $N \approx 24L^3$, and the truncated matrix \mathbb{W} is of the size $N \times N$. The algebraic complexity of a direct algebraic method such as LU decomposition to solve (30) is $O(N^3) = O(24^3 L^9)$. For the modest value $L = 50$ (corresponding to $\approx 10^6$ plane waves), we have $N \sim 3 \cdot 10^6$ and the computational complexity of $O(3 \cdot 10^{19})$, which is clearly out of reach. The generic complexity of an iterative method such as the conjugate-gradient descent⁵ or the continued-fraction expansion proposed above is $O(MN^2) = O(24^2 L^6 M)$, where M is the number of iteration. For $L = 50$ we obtain the complexity of $O(9 \cdot 10^{12} M)$. This is perhaps manageable on a supercomputer but is too much for typical applications.

We now utilize the separability of $M(\mathbf{g})$. Let us assume that we know some generic vector $|\mathbf{u}\rangle$ and wish to compute $|\mathbf{v}\rangle = \mathbb{W}|\mathbf{u}\rangle$. In components, we have

$$\langle \mathbf{g}\alpha | \mathbf{v} \rangle = \sum_{\mathbf{p}\beta} \langle \mathbf{g}\alpha | \mathbb{W} | \mathbf{p}\beta \rangle \langle \mathbf{p}\beta | \mathbf{u} \rangle \quad (41a)$$

$$= \sum_{\beta} K_{\alpha\beta}(\mathbf{q} + \mathbf{g}) \sum_{\mathbf{p}} M(\mathbf{g} - \mathbf{p}) \langle \mathbf{p}\beta | \mathbf{u} \rangle \quad (41b)$$

$$= \sum_{\beta} K_{\alpha\beta}(\mathbf{q} + \mathbf{g}) \langle \mathbf{g}\beta | \mathbf{u}_1 \rangle, \quad (41c)$$

where we have utilized (34c) for \mathbb{W} and

$$\langle \mathbf{g}\alpha | \mathbf{u}_1 \rangle = \sum_{\mathbf{p}} M(\mathbf{g} - \mathbf{p}) \langle \mathbf{p}\alpha | \mathbf{u} \rangle. \quad (42)$$

The complexity of computing $|\mathbf{v}\rangle$ from $|\mathbf{u}_1\rangle$ according to (41c) is $O(72L^3)$, which is negligible. The problem therefore is to compute $|\mathbf{u}_1\rangle$ from $|\mathbf{u}\rangle$ according to (42). Using (8), we have

$$\begin{aligned} \langle n_x n_y n_z \alpha | \mathbf{u}_1 \rangle &= \sum_{m_x=-L}^L M_x(n_x - m_x) \sum_{m_y=-L}^L M_y(n_y - m_y) \\ &\times \sum_{m_z=-L}^L M_z(n_z - m_z) \langle m_x m_y m_z \alpha | \mathbf{u} \rangle. \end{aligned} \quad (43)$$

⁵The matrix in question is not positive definite but we can use one of the several modifications of the conjugate-gradient method for complex symmetric matrices, i.e. see Ref. [28].

Here we have used the triplet of integers (n_x, n_y, n_z) in place of \mathbf{g} and (m_x, m_y, m_z) in place of \mathbf{p} . The complexity of this nested summation is $O(144L^4)$, and it is the dominating contribution in the case of separable $M(\mathbf{g})$. To obtain this result, we can break (43) into three independent summations. For example, we can write

$$\begin{aligned} \langle n_x n_y n_z \alpha | u_1 \rangle &= \sum_{m_x=-L}^L M_x(n_x - m_x) \\ &\times \sum_{m_y=-L}^L M_y(n_y - m_y) \langle m_x m_y n_z \alpha | u_2 \rangle, \end{aligned} \quad (44)$$

where

$$\langle n_x n_y n_z \alpha | u_2 \rangle = \sum_{m_z=-L}^L M_z(n_z - m_z) \langle n_x n_y m_z \alpha | u_1 \rangle. \quad (45)$$

We can further break (44) into two independent summations of the form (45). The complexity of each summation (45) is $O(48L^4)$ (the factor of 48 is $3 \cdot 2^4$), and we need three such summations to compute (43). This results in the overall complexity of $O(144L^4)$ as noted above. Again, using $L = 50$ as an example, we obtain the complexity of one matrix-vector multiplication of $9 \cdot 10^8$. In this particular case, the computational speed-up relative to the case of a generic \mathbb{W} is four orders of magnitude. For larger L , the speed-up is even more dramatic.

The above estimates were obtained for a cubic box of RLVs. We can easily generalize to the case of a rectangular box of the size $(2L_x + 1)(2L_y + 1)(2L_z + 1)$ where L_x, L_y and L_z are different integers. In a practical application, the values of L_x, L_y and L_z can be fine-tuned to provide convergence and optimal computational complexity. We finally note that numerical summation of the form (45) is easily parallelizable on computer architectures with shared memory or clusters.

5. Polarization modes

In Section 4, we have explained how the matrix $\Sigma(\mathbf{q})$ can be computed for an arbitrary argument \mathbf{q} . In order to find the Bloch wave vectors \mathbf{q}_B at a given frequency, we also need to solve the nonlinear equation (17). The latter is one complex equation for three complex Cartesian components $q_\alpha = q'_\alpha + i q''_\alpha$ ($\alpha = x, y, z$). Considering the electromagnetic frequency ω as one coordinate and q'_α, q''_α as six additional coordinates, and given the two constraints provided by (17), the set of solutions to the dispersion equation is a five-dimensional variety. Complete characterization of this variety is a complicated task. However, we can simplify the problem by restricting the values of \mathbf{q} in several ways.

One practically-relevant approach is to fix the projection of \mathbf{q} onto the XY plane [13, 25]. We write $\mathbf{q} = (k_x, k_y, q_z)$, where k_x and k_y are two known real constants and q_z is a complex scalar to be determined. Note that k_x and k_y can be defined by the boundary conditions at the interface $z = 0$ between the PC and another medium. That is, if a plane

wave with a real wave vector \mathbf{k} is incident onto a PC slab from vacuum, then k_x and k_y are projections of \mathbf{k} onto the X and Y axes. With the above restriction, (17) provides one complex equation for q_z . The solutions can be parameterized as $q'_{Bz}(\omega)$ and $q''_{Bz}(\omega)$ and therefore form a one-dimensional variety (usually, a curve, or several disjoint curves) in the three-dimensional space (ω, q'_z, q''_z) .

With the above restriction on \mathbf{q} , and for any finite truncation of $\mathbb{W}(\mathbf{q})$, the dispersion equation (17) is a polynomial in q_z , and therefore it has many roots. We are however interested only in solutions that are in the first Brillouin zone of the PC, and have tacitly assumed that k_x, k_y satisfy this condition. Then one can hope to solve (17) iteratively starting from the initial guess $q_z = 0$ without finding all the roots. Thus, we intend to replace a general eigenproblem with a relatively simple search for the root of (17) in the first Brillouin zone. To this end, we need to write (17) in a form that can be directly iterated⁶. This can be accomplished by noticing that the diagonal elements of Σ approach a finite limit when $q_z \rightarrow 0$. However, the off-diagonal elements with one of the indexes equal to “z” approach zero. Generally, the dependence of the off-diagonal elements on the components of \mathbf{q} is bilinear near $\mathbf{q} = 0$. We can write without loss of generality

$$\Sigma_{\alpha\beta}(\mathbf{q}) = \sigma_{\alpha\beta}(\mathbf{q}) \frac{q_\alpha q_\beta}{k^2}, \quad \alpha \neq \beta, \quad (46)$$

where $\sigma_{\alpha\beta}(\mathbf{q})$ approach finite limits when $\mathbf{q} \rightarrow 0$. Now we can use (46) together with the restriction $\mathbf{q} = (k_x, k_y, q_z)$ to reduce (17) to the following form:

$$A(\mathbf{q})q_z^4 + B(\mathbf{q})q_z^2 + C(\mathbf{q}) = 0. \quad (47)$$

The coefficients in this equation are given by the following expressions:

$$A = k^2 \eta_z + k_x^2 (\xi_{xz}^2 - 1) + k_y^2 (\xi_{yz}^2 - 1), \quad (48a)$$

$$\begin{aligned} B = & - \left[(\eta_x + \eta_y) k^2 - k_x^2 - k_y^2 \right] \left(\eta_z k^2 - k_x^2 - k_y^2 \right) \\ & - k_x^2 (\eta_y k^2 - k_x^2) \xi_{xz}^2 - k_y^2 (\eta_x k^2 - k_y^2) \xi_{yz}^2 \\ & + 2k_x^2 k_y^2 \xi_{xy} \xi_{xz} \xi_{yz}, \end{aligned} \quad (48b)$$

$$\begin{aligned} C = & \left[(\eta_x k^2 - k_y^2) (\eta_y k^2 - k_x^2) - k_x^2 k_y^2 \xi_{xy}^2 \right] \\ & \times \left(\eta_z k^2 - k_x^2 - k_y^2 \right), \end{aligned} \quad (48c)$$

where

$$\eta_\alpha = \langle \epsilon \rangle + \epsilon_h \chi \Sigma_{\alpha\alpha}, \quad (48d)$$

$$\xi_{\alpha\beta} = 1 + \epsilon_h \chi \Sigma_{\alpha\beta}, \quad \alpha \neq \beta. \quad (48e)$$

⁶Such a transformation is not generally required to solve (17), but is convenient if one wishes to obtain a few initial points that can be further used in the secant or rational interpolation methods.

The dependence of $\eta_\alpha, \xi_{\alpha\beta}$ on \mathbf{q} is implied⁷. We emphasize that (47) is not a quadratic equation. However, we can solve it as a quadratic equation formally for q_z^2 and thus transform it to a form suitable for fixed-point iteration. Alternatively, we can use some other iterative method such as Newton's, secant, or rational interpolation. The first two fixed-point iterations can be used to define the initial values for the secant or the rational interpolation methods. Also note that the quantities $\eta_\alpha(0) = \lim_{\mathbf{q} \rightarrow 0} \eta_\alpha(\mathbf{q})$ are the principal values of the effective permittivity of the medium in the homogenization limit [23]. At non-zero \mathbf{q} , the functions $\eta_\alpha(\mathbf{q})$ do not have a simple physical interpretation. The off-diagonal functions $\xi_{\alpha\beta}(\mathbf{q})$ do not appear in the theory of homogenization.

From the structure of (47), it is clear that it has two roots q_z^2 with q_z in the first Brillouin zone of the PC. These roots can be distinct and correspond to different *polarization modes*. By a polarization mode we mean here the amplitude of the fundamental Bloch harmonic \mathbf{E}_0 , which is a non-trivial solution to (16). In the general case, the polarization modes are quite complicated. Some simplifications can be obtained for special directions of propagation as discussed below. Note that, in order to define the polarization mode completely, we must choose the branch of the square root (of q_z^2). This corresponds to the fact that a Bloch wave can propagate in two opposite directions, and the polarization modes depend on the propagation direction. These counter-propagating modes correspond to different choice of sign in $\pm q_z$ and are related to each other by reflection in the XY plane.

Once the interaction tensor $\Sigma(\mathbf{q})$ is found for some \mathbf{q} , computing the coefficients of (47) according to the definitions (48a), (48b) and (48c) is straightforward but involves somewhat lengthy expressions. While evaluating these expressions numerically does not pose any problems or additional complexity, one may wish to obtain formulas that are easier to analyze. Cubic symmetry results in some simplification since, in this case, one can write $\eta_\alpha = \eta$ and $\xi_{\alpha\beta} = \xi$, so that the number of variables is reduced. However, the most significant simplifications are obtained for special propagation directions. These cases are discussed next.

5.1. Propagation in a crystallographic plane

Formulas are significantly simplified if we consider propagation in one of crystallographic planes XZ or YZ . For example, if we take $k_y = 0$, then \mathbf{q} lies entirely in the XZ plane. Equation (47) simplifies in this case to the following. For s -polarization:

$$q_z^2 = k^2 \eta_y - k_x^2, \quad (49a)$$

$$\mathbf{E}_0 = (0, 1, 0) \mathcal{E}; \quad (49b)$$

and for p -polarization:

$$q_z^2 = \frac{k^2 \eta_x (k^2 \eta_z - k_x^2)}{k^2 \eta_z - k_x^2 + \xi_{xz}^2 k_x^2}, \quad (49c)$$

⁷The quantities $\eta_\alpha, \chi_{\alpha\beta}$ and therefore A, B, C are functions of all three components of $\mathbf{q} = (k_x, k_y, q_z)$. This dependence must be accounted for when computing Σ and then A, B and C according to (48). However, k_x and k_y can be viewed as fixed parameters in the context of this paper.

$$\mathbf{E}_0 = (k^2 \eta_z - k_x^2, 0, -\xi_{xz} k_x q_{Bz}) \mathcal{E}, \quad (49d)$$

where \mathcal{E} is an arbitrary amplitude and q_{Bz} in (49d) is the solution to (49c). For the s -polarized mode, the amplitude of the fundamental Bloch harmonic is aligned with the Y -axis. Since \mathbf{q} is constrained to the XZ plane, this mode is transverse. The p -polarized mode is more complicated and generally neither transverse nor similar to the p -mode in a homogeneous anisotropic crystal. However, the analogy with the latter is restored in the low-frequency limit $k \rightarrow 0$. Indeed, as will be shown below, the nonzero off-diagonal values of $\sigma_{\alpha\beta}$ is a dynamic effect. That is, at low frequencies, $\sigma_{\alpha\beta}$ vanish and it follows from (48e) that $\xi_{\alpha\beta} \rightarrow 1$. From this we find for the p -polarized mode in the limit $k \rightarrow 0$:

$$q_z^2 = k^2 \eta_x - k_x^2 \frac{\eta_x}{\eta_z}, \quad (49e)$$

$$\mathbf{E}_0 = (k^2 \eta_z - k_x^2, 0, -k_x q_{Bz}) \mathcal{E}. \quad (49f)$$

This polarization mode is transverse in the sense that $k_x \eta_x E_{0x} + q_{Bz} \eta_z E_{0z} = 0$.

5.2. Propagation along crystallographic axes

Without loss of generality, we can consider propagation along the Z -axis. We set in this case $k_x = k_y = 0$ and obtain simple dispersion equations and polarization modes of the form

$$q_z^2 = k^2 \eta_x, \mathbf{E}_0 = (1, 0, 0) \mathcal{E} \quad (X\text{-polarization}), \quad (50a)$$

$$q_z^2 = k^2 \eta_y, \mathbf{E}_0 = (0, 1, 0) \mathcal{E} \quad (Y\text{-polarization}). \quad (50b)$$

For normal propagation (along the Z -axis), the modes cannot be classified as s - or p -polarized; instead, we say that the modes are X - or Y -polarized. These two polarizations are not generally equivalent. However, it can be seen that both polarization modes in (50a),(50b) are transverse.

6. Numerical examples

As in all numerical methods involving finite approximations of infinite mathematical objects, we must establish convergence of results with the truncation order(s). For the method introduced in this paper, there are three parameters that control convergence: the size of the box of RLVs, L , the truncation order of the continued fraction (39), N_{CF} , and the number of iterations needed to solve the nonlinear equation (47) with required precision, N_{iter} . The parameter L has been introduced in Sec. 4 when we discussed computational complexity. Establishing convergence with L is critical as the computational complexity of the method scales as L^4 but is linear in N_{CF} and N_{iter} .

In Fig. 1, we illustrate convergence of the interaction tensor Σ with L using the following model media. We consider a cubic elementary cell of the size $h_x = h_y = h_z = h$ containing a centered parallelepiped-shaped inclusion with the sides $2a_x = 2a_y = 0.8h$ and $2a_z = 0.5h$. Thus, the volume fraction of inclusions is $\rho = 0.32$. The working frequency ω used in Fig. 1 is such that $kh/\pi = 0.5$ or,

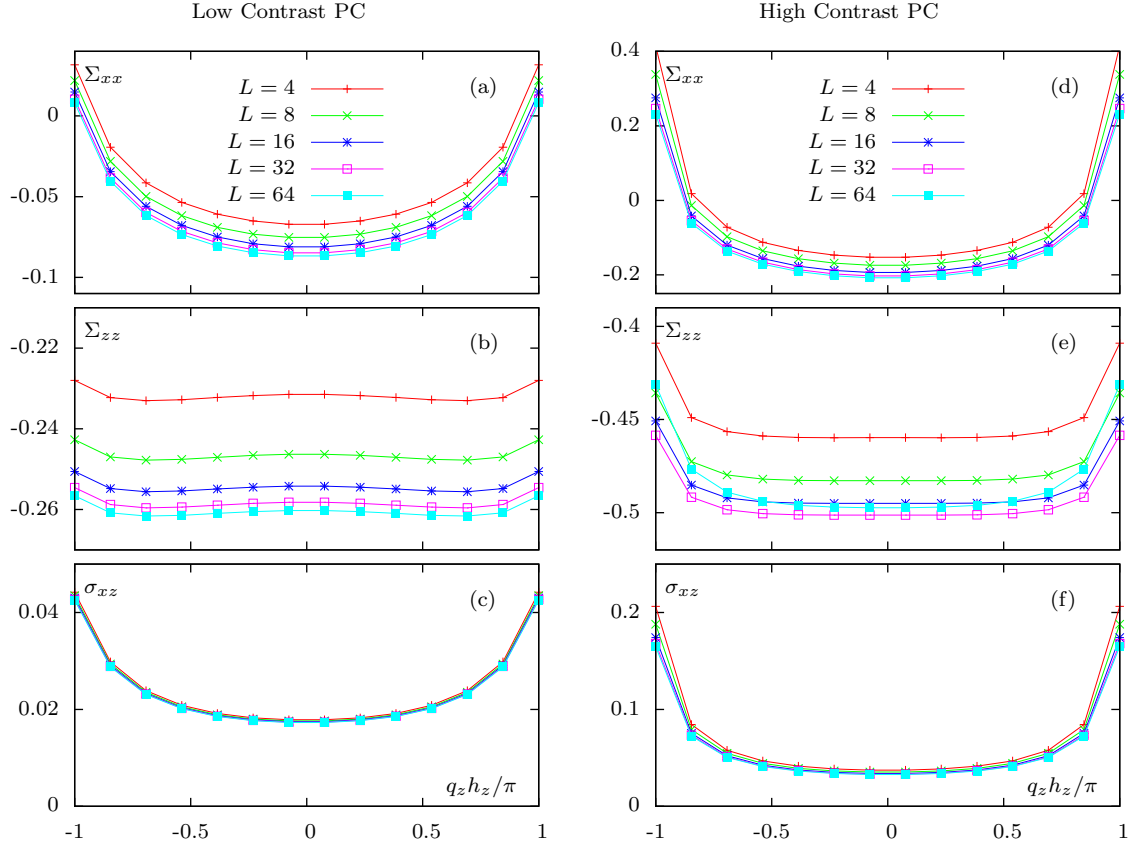


Figure 1: Convergence of the elements of interaction tensor Σ with the size of the box of RLVs (number of plane waves) L . Plots in the left and right columns correspond to the Low- and High-Contrast PCs, respectively. Propagation is in the XZ plane with fixed $k_x = 0.5k$, where $kh/\pi = 0.5$. Computations were carried out using truncation of continued fraction expansion (39) at the order $N_{CF} = 8$.

equivalently, $h = \lambda/4$, where k and λ are the free-space wave number and length. The propagation is in the XZ plane with $k_x = 0.5k$, which corresponds to 30° incidence angle for plane waves entering the PC from vacuum through the interface $z = 0$. The relevant elements of Σ in this case are Σ_{xx} , Σ_{zz} and $\Sigma_{xz} = (k^2/k_x q_z)\sigma_{xz}$ (see (46)). The host and inclusions are transparent dielectrics with $\epsilon_h = 2$ and $\epsilon_i = 4$ in one case (referred to as low-contrast PC) and $\epsilon_h = 2$, $\epsilon_i = 8$ in another case (high-contrast PC). Under the circumstances, the wave number q_{Bz} is real in the pass bands and imaginary in the band gaps⁸. Assuming the frequency is in the pass band, it is sufficient to seek the solution to (47) over reals. Therefore, we plot in (1) the elements of Σ as functions of real q_z . The truncation order of the continued fraction expansion N_{CF} is fixed and equal to 8 in these simulations. It can be seen that convergence with L is quite fast, at least for dielectric PCs. Converged results are reached at $L = 64$ for all cases considered and the results are already quite accurate at $L = 32$. In the special case of propagation strictly along the Z -axis, the only relevant element of Σ is Σ_{xx} , and for this element $L = 16$ is sufficient. Of course, we

⁸Above the second band gap of the high-contrast PC, there exist evanescent modes with more general complex q_{Bz} ; these modes can be considered separately.

should keep in mind that in higher bands larger values of L may be required.

In Fig. 2, we illustrate convergence of the continued fraction expansion (in this Figure, we have used $L = 64$). The truncation order N_{CF} is defined as the largest value of n in the expansion (39). In other words, we truncate the continued fraction by assuming that $\mu_n = 0$ for all $n > N_{CF}$. It can be seen that convergence of the continued fraction is fast, although it can be oscillatory. In all cases considered, the results with $N_{CF} = 16$ and $N_{CF} = 32$ are visually indistinguishable. For the low-contrast PC, the results with $N_{CF} = 8$ are already indistinguishable from those with $N_{CF} = 16$.

We next illustrate the dependence of Σ on frequency. In Fig. 3, we plot all four independent elements of $\Sigma(\mathbf{q} = 0)$ as functions of the free-space wave number k . The independent elements include $\Sigma_{xx} = \Sigma_{yy}$, Σ_{zz} , Σ_{xy} and $\Sigma_{xz} = \Sigma_{yz}$. Note that the off-diagonal elements are zero at $\mathbf{q} = 0$. We therefore display the derivatives $\sigma_{\alpha\beta}$, which are defined in (46). To compute the derivative, we have considered small but non-zero values of k_x and k_y . It can be seen that non-zero values of the off-diagonal terms $\sigma_{\alpha\beta}$ is, indeed, a dynamic effect, which disappears in the limit $kh \rightarrow 0$.

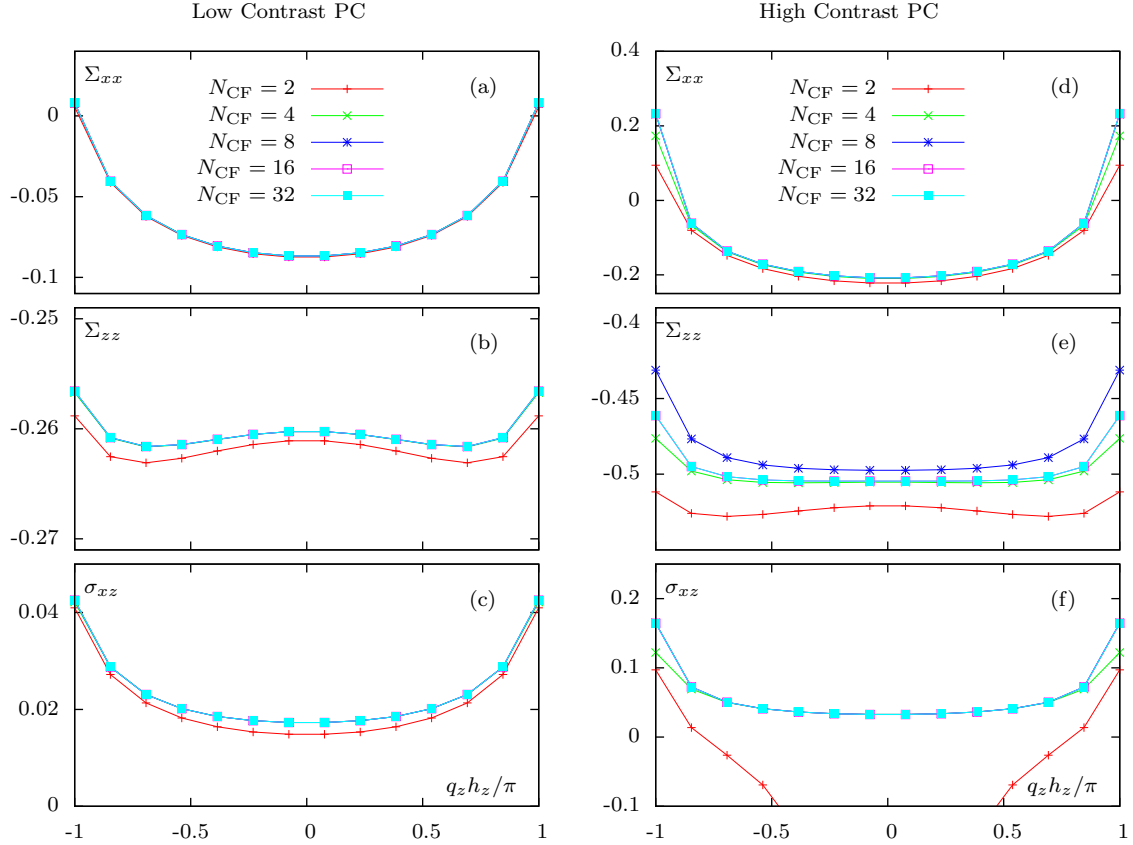


Figure 2: Convergence of the elements of interaction tensor Σ with the continued fraction truncation order N_{CF} for fixed $L = 64$. Same parameters as in Fig. 1.

The numerical methods used in this paper for solving the nonlinear equations (47) or one of its simplified forms are described in Appendix A and include fixed-point iteration, rational approximation, and various combinations of the two methods. Here we illustrate the application of these methods to computing dispersion curves. We start with purely real ϵ_i and ϵ_h , which is a more difficult case for us for the reasons that will become clear momentarily. In Fig. 4, we plot the dispersion diagram computed by fixed-point iteration starting from zero initial guess for the high-contrast PC with the same parameters as in Fig. 1. Propagation is strictly along the Z -axis and the polarization is along X . The equation that must be solved in this case is the first equation in (50a). The relative precision of $\epsilon = 10^{-4}$ was achieved for all points shown in the figure. At the frequencies for which no data points are shown (primarily, in the band gaps), convergence was not achieved. The difficulty mentioned above, is the following: a fixed point iteration with real ϵ_i and ϵ_h , which starts from a real initial guess, does not produce any imaginary or complex-valued solutions⁹. Therefore, a naive application of the fixed-point iteration method will produce the real Bloch wave numbers q_{Bz} in the pass bands but not the complex q_{Bz} in the gaps, nor

⁹Except if the argument of the square root becomes negative, which usually either does not occur or occurs in diverging iterations.

more complex evanescent modes that were mentioned in footnote 8. This is indeed what we see in the figure. Note that a few data points near the right edge of the plot (with $kh/\pi \approx 1$) correspond to an evanescent mode. However, in the pass bands, the convergence is fast, with only two or three iterations necessary to reach the precision specified above. Slightly more iterations are required close to the band gap edges.

The vertical lines in Fig. 4 indicate several special frequencies, for which the equation $q_z = f(q_z)$ (see Appendix A for details) is illustrated graphically in Fig. 5. It can be seen that, in the first pass band, the fixed-point iteration is expected to converge fast. In the second pass band, the function $f(q_z)$ is not continuous (there is a pole) and the iteration can diverge if started with a wrong initial guess. In practice, the fixed-point iteration still converged from zero initial guess in the second pass band as well. However, the existence of the pole indicates that the rational approximation is a better approach to root searching. For the two frequencies corresponding to the band gaps, there are no solutions to $q_z = f(q_z)$ over reals, and the iterations (either fixed-point or rational approximation) do not converge. This is the difficulty one encounters in the case of purely real permittivities.

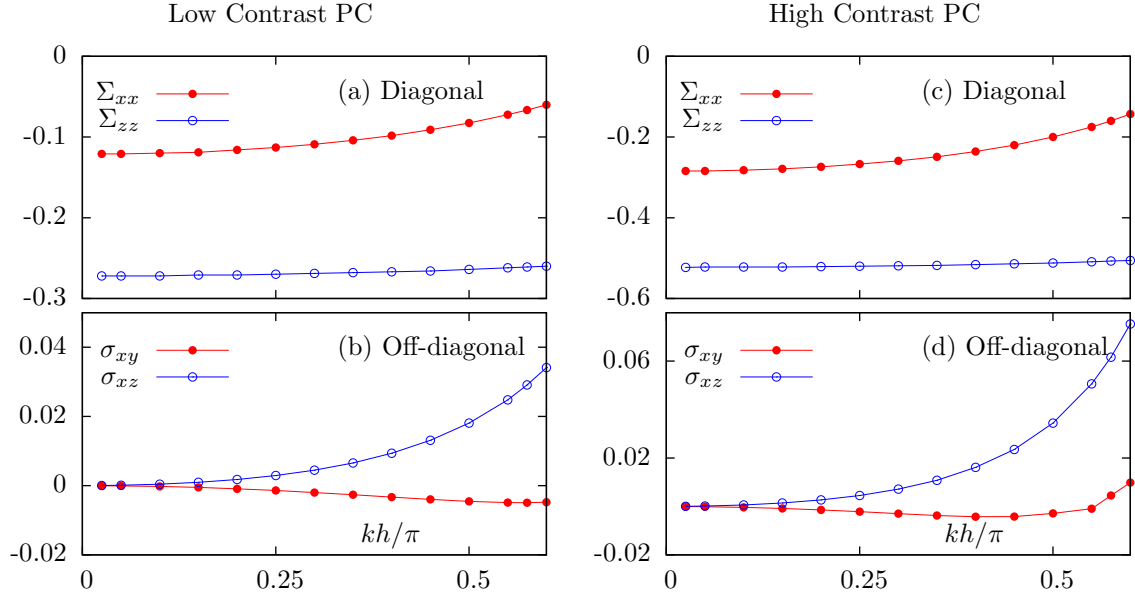


Figure 3: Dependence of the elements of Σ on $k = \omega/c$ at $\mathbf{q} = 0$. Small values of k_x and k_y were used to compute the derivative for the off-diagonal element σ_{xz} , according to (46). $L = 64$, $N_{\text{CF}} = 16$, other parameters same as in Figs. 1, 2.

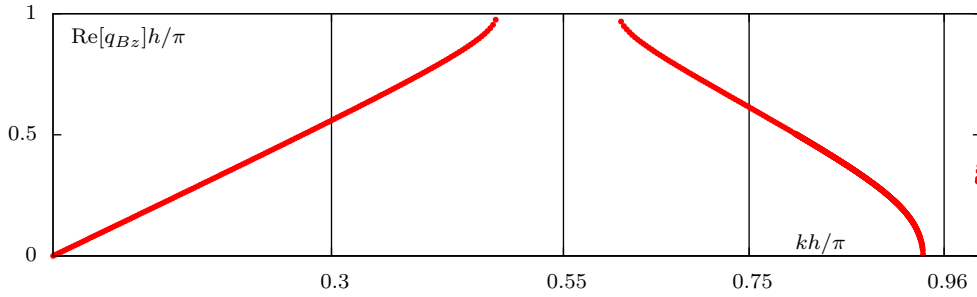


Figure 4: Real part of the Bloch wave number as a function of normalized frequency $kh/\pi = 2h/\lambda$ for the high-contrast PC ($\epsilon_h = 2$, $\epsilon_i = 8$, $h_x = h_y = h_z = h$, $a_x = a_y = 0.4h$, $a_z = 0.25h$). Propagation along the Z -axis with $k_x = k_y = 0$. Vertical lines show the frequencies for which the nonlinear equation $q_z = f(q_z)$ is illustrated graphically in Fig. 5 below.

In Fig. 6, we show how the complex solutions in the band gaps are formed. To obtain the data for this figure, we considered complex $q_z = q'_z + i q''_z$ and scanned the imaginary part q''_z for a fixed real part q'_z . We then plotted both the real and imaginary parts of the equation $q_z = f(q_z)$ and showed that both are satisfied at some value of q''_z . In Panel (a), we have fixed the frequency to $kh/\pi = 0.55$ (in the first band gap) and set $q'_z h/\pi = 1$. The imaginary part of the wave number was then scanned from 0 to $1/h$. It can be seen that around the value $q''_z = 0.39/h$, both parts of the equation $q_z = f(q_z)$ are simultaneously satisfied. This is indeed what we have found below in Fig. 8: the Bloch wave number at $kh/\pi = 0.55$ is $q_{Bz} \approx \pi/h + 0.3929i/h$. In panel (b) we illustrate how the root is formed in the second (narrow) band gap at $kh/\pi = 0.96$. In this case, the real part of the Bloch wave number is zero rather than π/h . Therefore the Bloch wave number is purely imaginary, $q_z = i q''_z$. As we scan q''_z from 0 to $1/h$, there is an interval in which

$f'(i q''_z) = 0$; the root obviously is constrained to this interval and determined by the second condition $q''_z = f''(i q''_z)$. This condition is satisfied at $q''_z \approx 0.82/h$. We note that the root-searching is somewhat difficult in this case because the function $f''(i q''_z)$ has a large derivative. However, the rational approximation algorithm still finds the root with good precision; in the solution $q''_z \approx 0.82/h$ all figures are significant; the error is in the next figure. This is indeed what can be seen in Fig. 8 below. We can also comment that the behavior of all functions in Panel (b) is that of a square root and the associated numerical instability of root-finding is that of computing the square root of a small number.

In principle, one can solve the dispersion equation in PCs with purely real permittivities by scanning either q'_z in the pass bands or q''_z in the band gaps. However, this approach requires determining whether a given frequency is in the pass band or in a gap, and also it is unclear how to proceed in the case of evanescent modes with more complicated q_z . Here

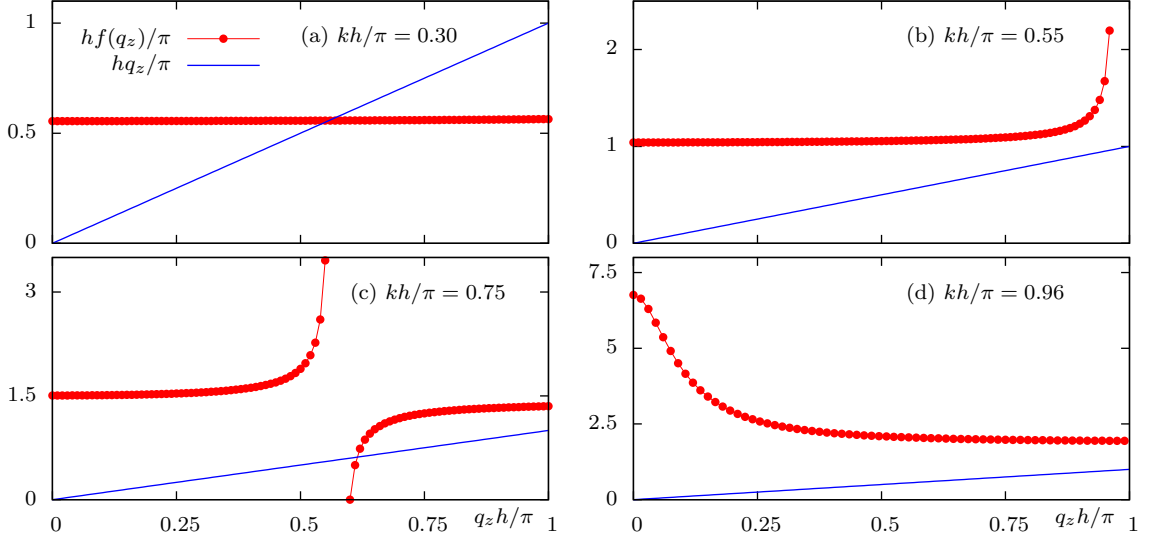


Figure 5: Graphical illustration of the equation $q_z = f(q_z)$, which was solved to obtain the data points shown in Fig. 4. Frequencies for which the four panels were computed correspond to the four frequencies indicated in Fig. 4 by vertical lines. The frequency (a) is in the first pass band, frequency (b) is in the first band gap, frequency (c) is in the second pass band and (d) is in the second band gap. For the frequencies in the band gaps, there are no solutions over reals.

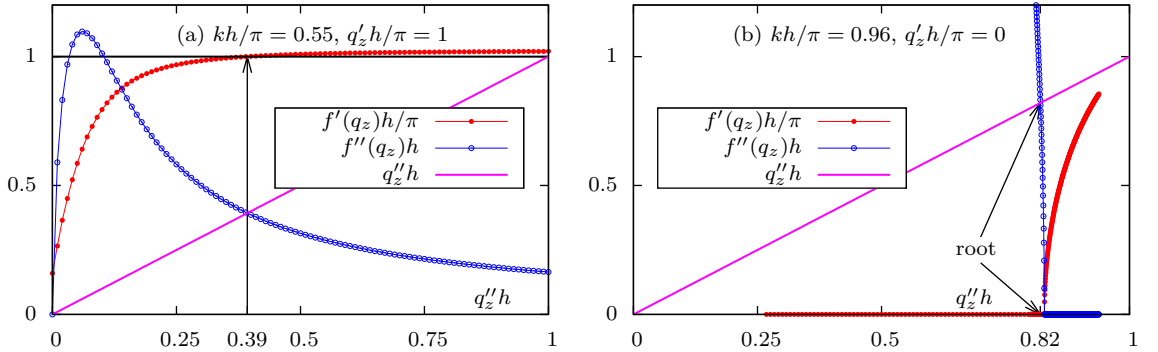


Figure 6: Graphical illustration of the equation $q_z = f(q_z)$, which was solved to obtain the data points shown in Fig. 4, at the frequencies inside the band gaps. In these plots, the real part q'_z of the wave number q_z is fixed as indicated and the imaginary part q''_z is scanned. The vertical arrows indicate the values of q''_z for which both parts of the equation $q_z = f(q_z)$ are satisfied simultaneously.

we adopt a different approach. We note that either fixed-point or rational approximation iteration work fine at all frequencies if the permittivities have some small but non-zero imaginary parts. This is illustrated in Fig. 7 where we show the dispersion relation for exactly the same PC as in Fig. 4 but with $\epsilon_i = 8 + 0.1i$ and $\epsilon_h = 2 + 0.02i$. Solutions at all frequencies were found easily with the simple fixed-point iteration (rational approximation yields the same result but faster). This observation suggests a general approach to solving the problem with purely real permittivities. Namely, we start with the fixed-point iteration and check whether a solution is found after some computationally reasonable number of iterations. If yes, we have found the solution and can move to the next frequency. If not, we modify slightly the permittivities by adding a small imaginary part

to them (typically, 0.1 of the absolute value of the real part is sufficient). We then find the solution with the modified permittivities using rational approximation. This can usually be obtained easily. At the next step, we roll back the permittivities to their original purely real values and use the just obtained complex solution as the initial guess for another rational approximation iteration. Since we start from a complex initial guess, which is not too far from the root, the iteration usually converges. We finally perform a shift to the first Brillouin zone and a precision correction if required as discussed in more detail in Appendix A.

Results of the above algorithm are illustrated in Fig. 8 where we plot both real and imaginary parts of q_z as functions of frequency for the high-contrast PC with purely real permittivities (same as in Fig. 4). A detailed frequency scan

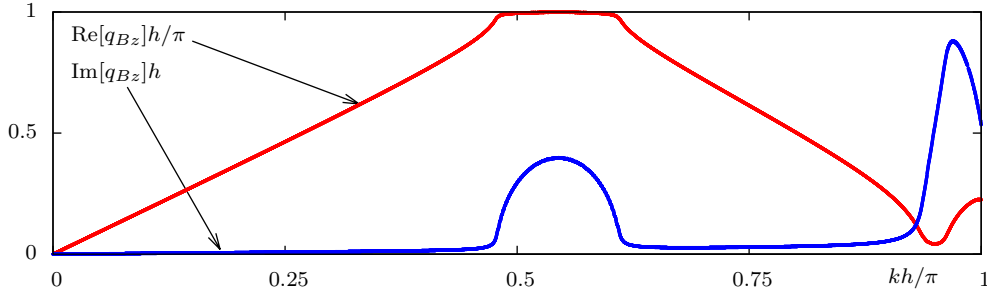


Figure 7: Same as in Fig. (4) but for complex permittivities $\epsilon_i = 8 + 0.1i$, $\epsilon_h = 2 + 0.02i$.

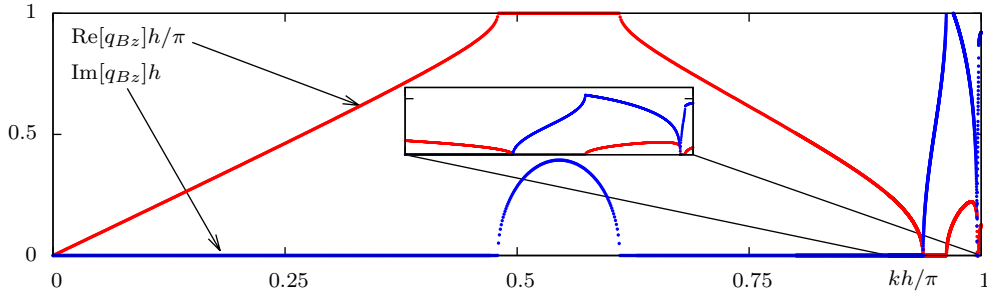


Figure 8: Same as in Fig. 4 but roots computed by a more advanced method as described in the text. The inset shows dispersion relation in the interval $0.9 < kh/\pi < 1$.

was performed with more than 2,000 independent frequency points. The algorithm converged with required precision at all these frequencies. The most difficult part was to compute the data in the second narrow band gap and the evanescent mode that follows immediately. These features are shown in the inset of the Figure. It can be seen that after the second pass band there is a narrow gap (the frequency $kh/\pi = 0.96$, which is considered in Fig. 6(b) is in this spectral interval). After the gap, there is an evanescent mode for which $q'_z \neq \pi/h, 0$ and $q''_z \neq 0$. After the evanescent mode there is another narrow band gap, which is hard to see in the inset due to the small width and then another evanescent mode. At higher frequencies, there are additional regular pass bands and band gaps (data not shown), which are actually not difficult to compute. However, at such high frequencies, the dispersion diagram becomes sensitive to the incidence angle and geometrical parameters of the PC.

To a large extent, the above discussion was focused on overcoming computational difficulties that one encounters in the case of purely real permittivities. However, the method of this paper is specifically designed for account of frequency dispersion, which in turn entails finite absorption. In fact, presence of absorption makes computations easier and the difficulties mentioned above are moot. From the physics standpoint, absorption suppresses strong multiple scattering and complicated electromagnetic resonances at high frequencies. This makes computations easier. The latter point is illustrated in Fig. 9 where we plot the number of iterations of the rational approximation solver that are required to achieve the stop condition $|F(q_z)| \leq 0.001$

(see Appendix A). Simulations were performed for the high contrast PC with added relatively small imaginary parts of the permittivities, ϵ''_h and ϵ''_i . It can be seen that, within the pass bands, the method converges fast independently of ϵ''_h and ϵ''_i (2 to 4 iterations is typical). However, near the edges of the pass bands and inside the band gaps, the required number of iterations increases and noticeably depends on ϵ''_h , ϵ''_i . As the latter quantities are increased, convergence becomes faster. Note that, if we set $\epsilon''_h = \epsilon''_i = 0$, the rational approximation method does not converge at some frequencies. The more complicated method described above still converges but is significantly slower. Thus, nonzero imaginary part of the permittivities is indeed advantageous for the proposed method.

In what follows, we show numerical examples for dispersive permittivities given by the following general formula:

$$\epsilon(\omega) = 1 + \frac{[\epsilon(0) - 1]\omega_0^2}{\omega_0^2 - \omega^2 - i\gamma\omega}. \quad (51)$$

Parameters for the host and inclusions are listed in Table 1. The frequency interval considered below is $0 < kh/\pi = \omega h/c\pi < 1$. The optical resonances in the two materials occur at significantly higher frequencies, which is typical for transparent dielectrics in the optical and infrared spectral ranges.

In Fig. 10 we show the dispersion curves for a PC whose constituents are described by equation (51) with parameters as specified in Table 1. The inclusion has the fixed width in the Z direction, $a_z = 0.25h$, and variable widths in the X and

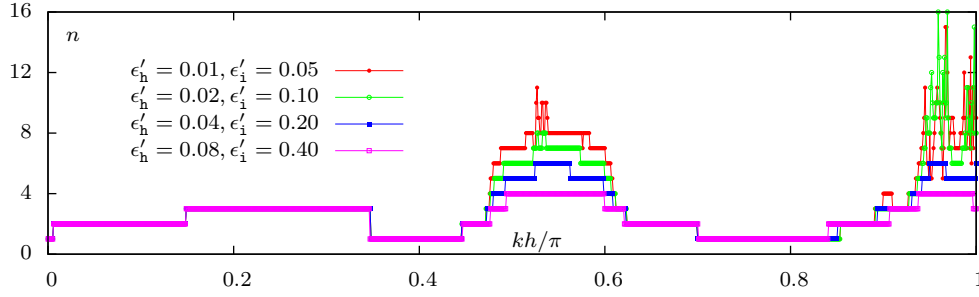


Figure 9: Number of iterations n of the rational approximation nonlinear solver required for achieving the stop condition $|F(q_z)| \leq 0.001$ (see Appendix A) for the same PC as in Fig. 7 but with small imaginary parts of the permittivities. The real parts $\epsilon'_h = 2$ and $\epsilon'_i = 8$ are fixed and the imaginary parts ϵ''_h and ϵ''_i are independent of frequency for each data set but vary between the data sets as labeled.

	$\epsilon(0)$	$\omega_0 h / \pi c = k_0 h / \pi = 2h / \lambda_0$	γ / ω_0
Host	2.0	3.0	0.01
Inclusions	8.0	2.0	0.10

Table 1

Optical parameters of host and inclusions used in dispersion formula (51). In the third column heading, $k_0 = \omega_0 / c$ and $\lambda_0 = 2\pi / k_0$, where c is the speed of light in vacuum.

Y directions, from $a_x = a_y = 0.1h$ to $a_x = a_y = 0.5h$. In the latter case, the PC is a one-dimensional layered medium in which the Bloch wave number can be found analytically. It can be seen that, in this case, the agreement between the theoretical and numerical results is almost perfect. It should be kept in mind that the numerical method is not reduced in this case to evaluating the theoretical formula; root searching is still required. As one can expect, the band gap is most pronounced in the case of layered medium and is suppressed as $a_x = a_y$ are decreased. At $a_x = a_y = 0.1$, there is no band-gap and the medium is quasi-homogeneous in the whole spectral range considered. The latter means that the dispersion of waves in such a medium is indistinguishable from that in a homogeneous medium with some effective parameters.

We finally demonstrate the method for different polarization modes when the propagation is not strictly along the Z -axis. To this end, we used the high-contrast PC with dispersion formula (51) and computed the dispersion for both s -polarized (Eq. (49a)) and p -polarized (Eq. (49c)) modes. It can be seen that the method works for off-normal propagation as well. Some high-frequency points were not computed (nonlinear solver failed to converge using default options) but this can be corrected by allowing longer run times. In general, we can always re-compute the data in the spectral intervals of interest with increased values of L , allowed number of iterations, etc. In the case of Fig. 11 the main spectral features are captured quite well and the displayed data points are accurate.

The figures in this section were computed using a workstation with 16 physical threads and efficient parallelization. Therefore, we have pushed the method to the limit and used,

for example, $L_x = L_y = L_z = 32$ for all frequencies, even though this is not really required. Many practical simulations can be performed with $L = 16$ or even $L = 8$. The computational package associated with this paper contains a demo directory with many examples of parameters files that can be used to compute realistic dispersion relations on an average laptop without parallelization; the timescale is two to three minutes for a thousand independent frequencies.

7. Validation

To validate the proposed method, we have performed a comparison with a conceptually-different numerical approach based on finite-element discretization of the field and Arnoldi iterations for the resulting polynomial equation. We have reproduced in this manner the data of Fig. 10. In this section, we briefly describe the alternative computation and present the comparison results.

To obtain a polynomial eigenproblem, we start from Maxwell's equation for the electric field, (9), and seek the solution using the ansatz $\mathbf{E}(\mathbf{r}) = e^{i\mathbf{q}\cdot\mathbf{r}}\tilde{\mathbf{E}}(\mathbf{r})$, where $\tilde{\mathbf{E}}(\mathbf{r})$ is the Bloch-periodic part of (10), that is, $\tilde{\mathbf{E}}(\mathbf{r}) = \sum_{\mathbf{g}} \mathbf{E}_{\mathbf{g}} e^{i\mathbf{g}\cdot\mathbf{r}}$. We however do not use the plane wave basis now but work directly with $\tilde{\mathbf{E}}(\mathbf{r})$, which is then projected onto the local finite-element basis. The strong formulation of the polynomial eigenvalue problem is obtained by substituting the above ansatz into (9) and canceling the common exponential factor $e^{i\mathbf{q}\cdot\mathbf{r}}$, which results in

$$-\mathbf{q} \times \mathbf{q} \times \tilde{\mathbf{E}} + i\mathbf{q} \times \nabla \times \tilde{\mathbf{E}} + i\nabla \times \mathbf{q} \times \tilde{\mathbf{E}} + \nabla \times \nabla \times \tilde{\mathbf{E}} - k^2 \epsilon \tilde{\mathbf{E}} = 0. \quad (52)$$

Here $\epsilon = \epsilon(\mathbf{r}, \omega)$ defined in Eqs. (1) and (2). The weak form is obtained by multiplying (52) with a test function \mathbf{V} and integrating the resulting equation over the unit cell \mathcal{C}

$$-\int_{\mathcal{C}} (\mathbf{q} \times \mathbf{q} \times \tilde{\mathbf{E}}) \cdot \mathbf{V} d^3r + i \int_{\mathcal{C}} (\mathbf{q} \times \nabla \times \tilde{\mathbf{E}}) \cdot \mathbf{V} d^3r + i \int_{\mathcal{C}} (\nabla \times \mathbf{q} \times \tilde{\mathbf{E}}) \cdot \mathbf{V} d^3r + \int_{\mathcal{C}} (\nabla \times \nabla \times \tilde{\mathbf{E}}) \cdot \mathbf{V} d^3r - k^2 \int_{\mathcal{C}} \epsilon \tilde{\mathbf{E}} \cdot \mathbf{V} d^3r = 0. \quad (53)$$

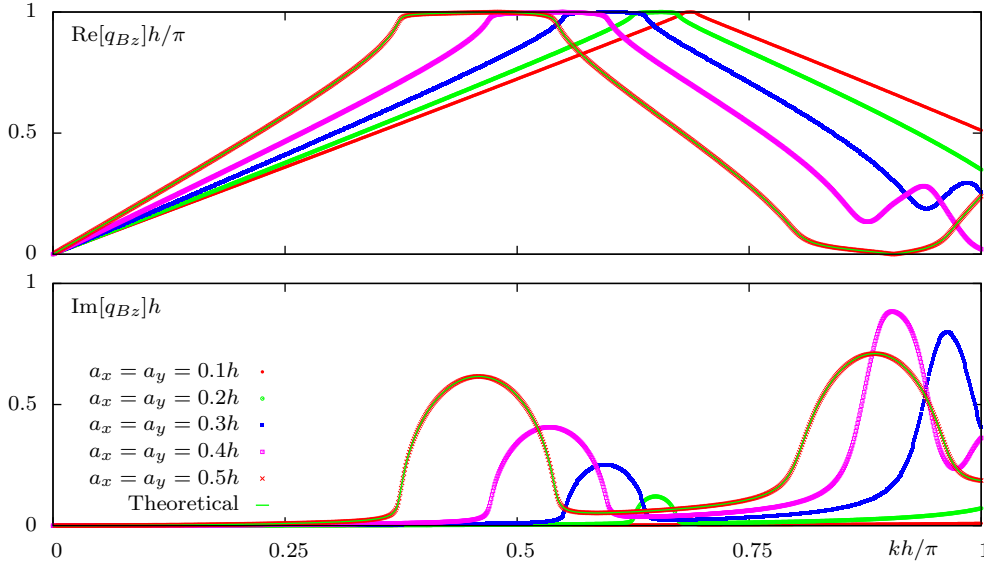


Figure 10: Real (top) and imaginary (bottom) parts of the Bloch wave number as functions of normalized frequency kh/π for the PCs with constituents described by the dispersion formula (51) with parameters specified in Table 1. Propagation along Z -axis, polarization along X or Y . Inclusions have fixed width $a_z = 0.25h$ and variable $a_x = a_y$ as labeled. When $a_x = a_y = 0.5h$, the PC is a layered medium, uniform in the X - and Y directions. In this case, a theoretical solution for q_{Bz} is available, and it is represented in the plots by a solid line. The agreement between numerical and theoretical results is sufficiently close so that the two data sets are not visually distinguishable.

Using integration by parts and elementary algebra, the differentiation orders can be split evenly between $\tilde{\mathbf{E}}$ and \mathbf{V} , so that (53) is written equivalently in the form

$$\begin{aligned} & \int_{\mathcal{C}} (\mathbf{q} \times \tilde{\mathbf{E}}) \cdot (\mathbf{q} \times \mathbf{V}) d^3r \\ & + i \int_{\mathcal{C}} [(\mathbf{q} \times \nabla \times \tilde{\mathbf{E}}) \cdot \mathbf{V} - \tilde{\mathbf{E}} \cdot (\mathbf{q} \times \nabla \times \mathbf{V})] d^3r \\ & + \int_{\mathcal{C}} (\nabla \times \tilde{\mathbf{E}}) \cdot (\nabla \times \mathbf{V}) d^3r - k^2 \int_{\mathcal{C}} \epsilon \tilde{\mathbf{E}} \cdot \mathbf{V} d^3r = 0. \end{aligned} \quad (54)$$

Note that the boundary integrals generated due to the integration by parts sum to zero as a result of the periodic boundary conditions.

We now specialize to the case of Bloch wave propagation along the Z -axis so that $\mathbf{q} = q_z \hat{\mathbf{z}}$, where q_z is a complex number to be found. We select the polarization mode along the X -axis by applying the auxiliary conditions

$$\int_{\mathcal{C}} \tilde{E}_y d^3r = 0, \quad \int_{\mathcal{C}} \tilde{E}_z d^3r = 0. \quad (55)$$

These conditions correspond to selecting the polarization mode $\mathbf{E}_0 = (1, 0, 0)^{\mathcal{E}}$ (see (50a) in Sec. 5.2). We have accounted for these conditions by introducing two spaces \mathcal{C} consisting of one global complex degree of freedom each, which are used to test the condition (55). For practical purposes, this auxiliary space \mathcal{C} can be identified with the field of complex numbers. Elements of these spaces, including their symmetric counterparts, are added to (54) to obtain a saddle-point problem. For discretization of $\tilde{\mathbf{E}}$, a second order

Nedelec space \mathcal{N} was used. Details of the finite element spaces and their implementation in Netgen/NGSolve [29] can be found in [30] and [31].

The numerical problem is then formulated as follows: Find $\tilde{\mathbf{E}} \in \mathcal{N}$ and $\eta_1, \eta_2, q_z \in \mathcal{C}$ such that

$$\begin{aligned} & q_z^2 \int_{\mathcal{C}} (\hat{\mathbf{z}} \times \tilde{\mathbf{E}}) \cdot (\hat{\mathbf{z}} \times \mathbf{V}) d^3r \\ & + i q_z \int_{\mathcal{C}} [(\hat{\mathbf{z}} \times \nabla \times \tilde{\mathbf{E}}) \cdot \mathbf{V} - \tilde{\mathbf{E}} \cdot (\hat{\mathbf{z}} \times \nabla \times \mathbf{V})] d^3r \\ & + \int_{\mathcal{C}} (\nabla \times \tilde{\mathbf{E}}) \cdot (\nabla \times \mathbf{V}) d^3r - k^2 \int_{\mathcal{C}} \epsilon \tilde{\mathbf{E}} \cdot \mathbf{V} d^3r \\ & + \int_{\mathcal{C}} (\xi_1 \tilde{E}_y + \xi_2 \tilde{E}_z + \eta_1 V_y + \eta_2 V_z) d^3r = 0. \end{aligned} \quad (56)$$

for all $\mathbf{V} \in \mathcal{N}$ and $\xi_1, \xi_2 \in \mathcal{C}$. Assembling (56) leads to the matrix equation

$$(q_z^2 A_1 + q_z A_2 + A_3) \mathbf{u} = 0, \quad (57)$$

where A_1, A_2 and A_3 are the finite element matrices, which depend on ω but not on q_z , and \mathbf{u} is the coefficient vector of projections of $\tilde{\mathbf{E}}$ onto the basis of the chosen finite element space. This equation is solved using a variant of Arnoldi iteration [32, Chapter 1] modified to handle the polynomial eigenvalue problem.

Results of the comparison are shown in Figs. 12 and 13. In these figures, we reproduce the dispersion curves shown in Fig. 10 and provide a detailed comparison of the data. As the two methods employed here are completely different, the obtained agreement is quite remarkable. The

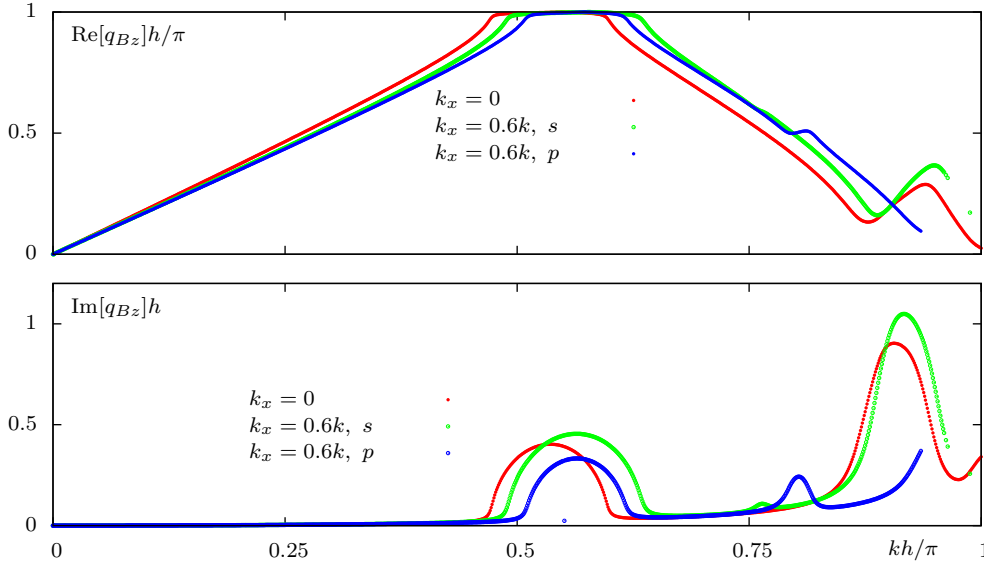


Figure 11: Same as in Fig. 10 but for fixed $a_x = a_y = 0.4h$ and propagation direction in XZ -plane. Two different polarization modes are shown. Polarization along Y is marked as s and polarization in the XZ -plane as p . The projection of Bloch wave number onto the X -axis is $k_x = 0.6k$ for all frequencies. The curve for normal propagation (identical to the curve with $a_x = a_y = 0.4h$ in Fig. 11) is shown for comparison. Some points close to the right edge of the plots were not computed with the default settings we used and not shown (nonlinear solver failed to converge) but can be found with additional effort/refining. The shown data points were verified by comparing $L_x = L_y = L_z = 16$ with $L_x = L_y = L_z = 32$ (no discernible difference).

slight deviations seen at higher frequencies are probably due to insufficient basis in one or both of the methods. We thus conclude that the results obtained by the proposed method are reliable under the condition that convergence of the numerical solver has been achieved.

8. Summary of the method

In this section we give a brief self-consistent summary of the proposed method. To avoid repetition, references are given to equations of the previous sections; however, the main definitions are repeated. We describe here the algorithm for one rectangular inclusion but it can be easily generalized for a direct superposition of several such inclusions, which can be used to define unit cells of more complicated shape.

The PC is assumed to have a rectangular geometry with the crystallographic axes coinciding with the axes of a Cartesian reference frame XYZ . The unit cell of the lattice is a cuboid of the dimension $h_x \times h_y \times h_z$. Each cell has one co-centric cuboidal inclusion of the size $2a_x \times 2a_y \times 2a_z$. Note that the dimensions of the cell and the inclusion are not required to be proportional. In other words, the ratios a_x/h_x , a_y/h_y and a_z/h_z are arbitrary modulo the geometrical limitation $a_\alpha/h_\alpha \leq 0.5$ ($\alpha = x, y, z$). If equality holds for some α , the inclusions are continuous in this direction and the problem dimensionality is effectively reduced.

The method computes the Cartesian component q_z of the Bloch wave vector $\mathbf{q} = (q_x, q_y, q_z)$ as a function of the electromagnetic frequency ω from the characteristic

equation $\det[\Pi(\mathbf{q})] = 0$, where $\Pi(\mathbf{q})$ is a 3×3 . In this paper and in the associated computer codes, $q_x(\omega)$ and $q_y(\omega)$ are specified and known, i.e., determined from the interface conditions while $q_z(\omega)$ is computed. However, the method can be used for other restrictions of the Bloch variety.

The matrix elements of $\Pi(\mathbf{q})$ are given by

$$\Pi_{\alpha\beta}(\mathbf{q}) = q_\alpha q_\beta + (k^2 \langle \epsilon \rangle - q^2) \delta_{\alpha\beta} + k^2 \epsilon_h \chi \Sigma_{\alpha\beta}(\mathbf{q}), \quad (58a)$$

where $\alpha, \beta = x, y, z$. In the above formula,

$$k = \frac{\omega}{c}, \quad \rho = \frac{8a_x a_y a_z}{h_x h_y h_z}, \quad \langle \epsilon \rangle = (1 - \rho)\epsilon_h + \rho\epsilon_i, \quad (58b)$$

$$\chi = \rho \frac{\epsilon_i - \epsilon_h}{\epsilon_h}. \quad (58c)$$

Here ω is the real-valued electromagnetic frequency, ρ is the volume fraction of inclusions, ϵ_h and ϵ_i are the possibly complex and dispersive permittivities of the host and inclusions, respectively, $\langle \epsilon \rangle$ is the average complex permittivity of the medium, χ is the complex coupling constant, and the 3×3 complex symmetric matrix $\Sigma(\mathbf{q})$ (the interaction tensor) is defined next.

The main part of the algorithm is computing the interaction tensor $\Sigma(\mathbf{q})$. Formally, the elements $\Sigma(\mathbf{q})$ are defined as a resolvent of the matrix $\mathbb{W}(\mathbf{q})$,

$$\Sigma_{\alpha\beta}(\mathbf{q}) = \left\langle \mathbf{a}^{(\alpha)} \left| \left[\chi^{-1} \mathbf{I} - \mathbb{W}(\mathbf{q}) \right]^{-1} \right| \mathbf{b}^{(\beta)}(\mathbf{q}) \right\rangle, \quad (59)$$

where \mathbf{I} is a unit tensor and the vectors $|\mathbf{a}^{(\alpha)}\rangle$, $|\mathbf{b}^{(\beta)}(\mathbf{q})\rangle$ and the matrix $\mathbb{W}(\mathbf{q})$ are defined in Eqs. (34). Elements of the

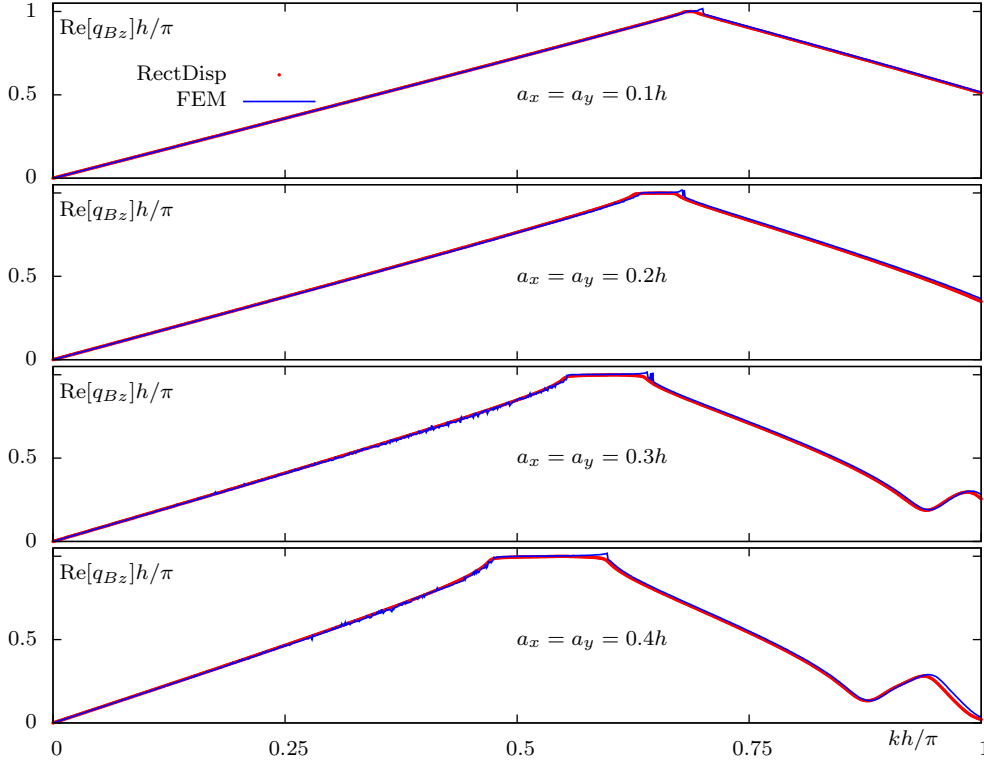


Figure 12: Comparison of the real part of the Bloch wave number q_{Bz} as a function of the normalized frequency computed by the method of this paper using the package RectDisp (red centered symbols labeled as RectDisp) and by finite element discretization and Arnoldi iterations (blue line labeled as FEM), as described in Section 7. Computations are shown for the same geometry and PC parameters as in Fig. 10. Permittivities of the host and inclusions are given by (51) with the parameters as shown in Table 1. The case $x_a = a_y = h/2$ is not shown as both methods reproduce in this case the analytical result with high precision.

vectors $|\mathbf{a}^{(\alpha)}\rangle$, $|\mathbf{b}^{(\beta)}(\mathbf{q})\rangle$ and of the matrix $\mathbb{W}(\mathbf{q})$ are labeled by a composite index consisting of $\gamma (= x, y, z)$ and by the RLVs $\mathbf{g} = 2\pi(n_x/h_x, n_y/h_y, n_z/h_z)$ where n_α are integers in the range $-L_\alpha \leq n_\alpha \leq L_\alpha$ and the trivial vector $\mathbf{g} = \mathbf{0}$ is excluded. Here L_α are truncation parameters that determine the size of the RLV box used in the simulations. The total length of the vectors (the number of plane waves used) is $3(2L_x + 1)(2L_y + 1)(2L_z + 1) - 1$. In many cases, one can take $L_x = L_y = L_z = L$. However, if inclusions are continuous in the direction α (if $a_\alpha = h_\alpha/2$), it is sufficient to take $L_\alpha = 0$.

Although the size of $\mathbb{W}(\mathbf{q})$ can be rather large, computation of the resolvent in (59) is achieved efficiently by the iterative method which takes advantage of the fact that $\mathbb{W}(\mathbf{q})$ is a product of a block-diagonal matrix (with blocks of the size 3×3) and a separable matrix. This decomposition is evident in the explicit form (34c). The problem here is that of algebra for matrices of a special form; Section 4 gives a complete description of the method for computing the resolvent in (59) and an estimate of computational complexity. For a three-dimensional problem (without dimensionality reduction due to continuity of inclusions), the latter scales as ML^4 where L is the size of RLV box as defined above and M is the number of iterations (typically, $M = 16$ is sufficient). This complexity is a very significant reduction from L^9 for direct

methods or ML^6 for iterative methods that do not account for the special properties of the matrices involved.

9. Discussion

The method of computing dispersion relations in PCs proposed in this paper is specialized but efficient for the narrow class of problems to which it applies. We have utilized the specific geometry of the problem by choosing the appropriate basis and exploiting variable separation. It should be noted that variable separation can be used for solving electromagnetic problems with many regular shapes. However, the only case when this works in three-dimensional periodic media such as PCs is rectangular geometry (in two dimensions, one can develop similar methods for triangular lattices with triangular inclusions). Still, rectangular geometry is frequently used in applications and PCs of this kind are easy to manufacture. The method can be generalized to several nested rectangular inclusions (with the same center) and thus allow inclusion of more than two materials.

The main idea on which this paper is based in reducing the eigenproblem of finding the Bloch wave vector to a nonlinear equation. The interaction tensor that appears in this procedure was introduced by us earlier in the context of homogenization theory [23–25]. Here we have shown that

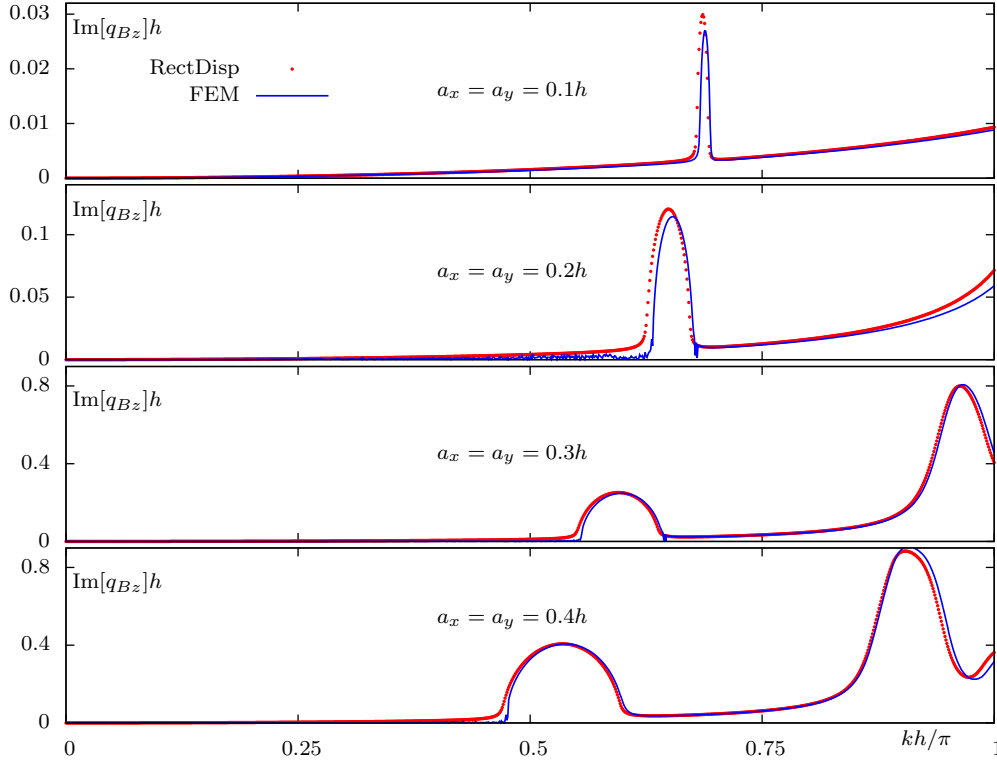


Figure 13: Same as in Fig. 12 but for the imaginary part of the Bloch wave number.

the interaction tensor can be computed efficiently within the iterative solver and that the iterations in many cases converge to the correct solution.

We have used Fourier basis to expand the field in the PC. This expansion is known to be only linearly converging. However, in order to compute the Bloch wave vector by the method of this paper, point-wise convergence of the field is not required. It can be said that we rely on a weak formulation of the eigenproblem. In many examples included with the computational package, selecting $L_\alpha = 8$ (~ 5000 plane waves) is sufficient for good accuracy as can be verified by doubling this number. Roughly, $L_\alpha = 16$ is doable on a laptop computer, $L_\alpha = 32$ and $L_\alpha = 64$ can be done on a good workstation with parallelization and $L_\alpha = 128$ or $L_\alpha = 256$ requires a supercomputer. Large number of plane waves is unlikely to be needed even in the case of sharp electromagnetic resonances which can occur in metal-dielectric PCs.

Of course, one can find cases when solution is difficult to find or the method is slow. This is always true at sufficiently high frequencies. It is clear intuitively that the higher the frequency is, the faster are field variations inside the material and the more basis functions one must utilize to capture the field behavior with sufficient accuracy. However, simulations shown in Section 6 indicate that the method is quite stable in the first few pass bands and band gaps and can capture complicated evanescent modes. We also note that computations in the pass bands are almost always faster

than in band gaps or evanescent mode bands. If all that one needs is the dispersion curves in the pass bands, these can be computed efficiently by limiting the number of allowed iterations to ~ 5 . This number can be controlled from the parameter file in the computational package associated with this paper.

We provide with this paper a complete computational package that implements the methods described above. One limitation of the current version of the codes is that they find at most one \mathbf{q} (not counting its negative, $-\mathbf{q}$) for any given frequency. In the first couple of pass bands and band gaps, this is usually enough, but at higher frequencies there can be multiple solutions (branching) [33]. Some of these additional solutions are spurious modes, which appear due to the so-called artificial band folding. In other words, these modes can be found by standard eigenvalue-seeking codes in an artificially-discretized homogeneous medium. Classification of the spurious mode is complicated and, at present, we do not have a systematic method to address it. We believe however that the method reported in this paper does not find the spurious modes as we work under the assumption that the amplitude of the fundamental Bloch harmonic \mathbf{E}_0 is not zero. For this reason, spurious modes are not coupled to external radiation and not excited in the actual PCs. Still, there can exist multiple solutions at a given frequency that are not spurious. Under most circumstances, such additional solutions appear at the frequencies $kh/\pi \gtrsim 1$. If the proposed method is used, an apparent loss of continuity of the dispersion curve

(random jumps) can be an indication of multiple solution. The high-frequency electromagnetic properties of PCs can be complicated and the code users should be cautious when working in the above spectral region. In the future releases, we plan to include the capability of searching multiple non-spurious solutions at any given frequency. One promising approach is to use Pade approximants for $\Sigma(\mathbf{q})$ (the coefficients can be computed by sampling \mathbf{q} at a sufficient number of points). Then the problem is reduced to a finite-number polynomial equation in \mathbf{q} ; the solutions can be refined if necessary to account for the imprecision of the Pade approximation.

Finally, we note that the method of this paper can be used directly to compute dispersion relations in two-dimensional or one-dimensional PCs (in the latter case, an analytical solution is available). Thus, to consider a two dimensional PC that is continuous in the X -direction, set $a_x = h_x/2$. We emphasize that the third dimension is still present; the PC is always a three-dimensional object, as is the case in reality. In particular, we can consider propagation in the XZ plane and the two polarization modes associated with this direction. In the case $a_x = h_x/2$, it is sufficient to select $L_x = 0$ and the code will run much faster. All these capabilities are implemented in the computational package.

Authors are grateful for I. Tsukerman for useful discussions.

References

- [1] M. A. Butt, S. N. Khonina, N. L. Kazanskiy, Recent advances in photonic crystal optical devices: A review, *Opt. Las. Techn.* 142 (2021) 107265.
- [2] A. H. Aly, A. Ahgajamali, H. A. Elsayed, M. Mobarak, Analysis of cutoff frequency in a one-dimensional superconductor-metamaterial photonic crystal, *Physica C* 528 (2016) 5–8.
- [3] A. H. Aly, C. Malek, H. A. Elsayed, Transmittance properties of a quasi-periodic one-dimensional photonic crystals that incorporate nanocomposite material, *Int. J. Mod. Phys. B* 32 (2018) 1850220.
- [4] A. H. Aly, H. A. Elsayed, Transmittance properties of one-dimensional metallic-dielectric photonic crystals in near-zero permittivity, *Physica Scripta* 94 (2019) 125501.
- [5] H. A. Elsayed, A. Mehaney, Theoretical verification of photonic crystals sensor for biodiesel detection and sensing, *Physica Scripta* 95 (2020) 085507.
- [6] Y. Zhang, B. Li, Photonic crystal-based bending waveguides for optical interconnections, *Opt. Expr.* 14 (2006) 5723–5732.
- [7] B. Liu, Y.-F. Liu, C. Jia, X.-D. He, All-optical diode structure based on asymmetrical coupling by a micro-cavity and fp cavity at two sides of photonic crystal waveguide, *AIP Advances* 6 (2016) 065316.
- [8] M. Noori, M. Soroosh, H. Baghban, Self-collimation in photonic crystals: Applications and opportunities, *Annalen Der Physik* 530 (2017) 1700049.
- [9] J. D. Joannopoulos, R. D. Meade, J. N. Winn, *Photonic Crystals: Molding the Flow of Light*, Princeton University Press, Princeton, N.J., 2008.
- [10] T. Suzuki, P. K. L. Yu, Tunneling in photonic band structures, *J. Opt. Soc. Am. B* 12 (1995) 804–820.
- [11] E. Istrate, A. A. Green, E. H. Sargent, Behavior of light at photonic crystal interfaces, *Phys. Rev. B* 71 (2005) 195122.
- [12] T. Suzuki, P. K. L. Yu, Complex photonic band structures of a conductive metal lattice by a quadratic eigensystem, *Opt. Lett.* 20 (1995) 2520–2522.
- [13] M. Saba, G. E. Schroeder-Turk, Bloch modes and evanescent modes of photonic crystals: Weak form solutions based on accurate interface triangulation, *Crystals* 5 (2015) 14–44.
- [14] Y. Brule, B. Gralak, G. Demesy, Calculation and analysis of the complex band structure of dispersive and dissipative two-dimensional photonic crystals, *J. Opt. Soc. Am. B* 33 (2016) 691–702.
- [15] C. Lackner, S. Meng, P. Monk, Determination of electromagnetic Bloch variety in a medium with frequency-dependent coefficients, *J. Comput. Appl. Math.* 358 (2019) 359–373.
- [16] J. B. Pendry, A. MacKinnon, Calculation of photon dispersion relations, *Phys. Rev. Lett.* 69 (1992) 2772–2775.
- [17] P. M. Bell, J. B. Pendry, L. M. Moreno, A. J. Ward, A program for calculating photonic band structures and transmission coefficients of complex structures, *Comp. Phys. Comm.* 85 (1995) 306–322.
- [18] K. Cho, J. Ushida, M. Bamba, Optical response of photonic crystals requiring high precision band calculation in the form of $k(\omega)$ including evanescent waves, *J. Phys. Soc. Jpn.* 74 (2005) 3088–3092.
- [19] Y.-C. Hsue, T.-J. Yang, Contour of the attenuated length of an evanescent wave at constant frequency within a band gap of photonic crystal, *Solid State Comm.* 129 (2004) 475–478.
- [20] Y. Ohtera, Calculating the complex photonic band structure by the finite-difference time-domain based method, *Jpn. J. Appl. Phys.* 47 (2008) 4827–4834.
- [21] M. A. Botchev, L. A. Knizhnerman, ART: Adaptive residual-time restarting for Krylov subspace matrix exponential evaluations, *J. Comput. Appl. Math.* 364 (2020) 112311.
- [22] T. M. Huang, W. Liao, W. W. Lin, W. Wang, An efficient contour integral based eigensolver for 3d dispersive photonic crystal, *J. Comput. Appl. Math.* 395 (2021) 113581.
- [23] V. A. Markel, J. C. Schotland, Homogenization of Maxwell's equations in periodic composites, *Phys. Rev. E* 85 (2012) 066603.
- [24] V. A. Markel, I. Tsukerman, Current-driven homogenization and effective medium parameters for finite samples, *Phys. Rev. B* 88 (2013) 125131.
- [25] V. A. Markel, I. Tsukerman, Applicability of effective medium description to photonic crystals in higher bands: Theory and numerical analysis, *Phys. Rev. B* 93 (2016) 224202.
- [26] J. Silvester, Determinants of block matrices, *Math. Gaz.* 84 (2000) 460–467.
- [27] P. D. Powell, Calculating determinants of block matrices, *arXiv:1112.4379* (2011).
- [28] M. Petracic, J. Kuo-Petravic, An ILUCG algorithm which minimizes in the Euclidean norm, *J. Comput. Phys.* 32 (1979) 263–269.
- [29] J. Schöberl, *Netgen/NGSolve*. URL <https://ngsolve.org/>
- [30] J. Schöberl, S. Zaglmayr, High order Nédélec elements with local complete sequence properties, *COMPEL* 24 (2005) 374–384.
- [31] S. Zaglmayr, High order finite element methods for electromagnetic field computation, Ph.D. thesis, Johannes Kepler Universität, Linz, Austria (2006).
- [32] Y. Saad, *Numerical Methods for Large Eigenvalue Problems*, SIAM, 2011.
- [33] T. Minami, H. Ajiki, K. Cho, Branching ratio of light incident on a photonic crystal in a multibranch dispersion region, *Physica E* 13 (2002) 432–436.

A. Numerical methods of solving (47)

Equation (47) is of the general form $F(z) = 0$, where z is a complex variable and

$$F(z) = A(z)z^4 + B(z)z^2 + C(z). \quad (60)$$

The functions $A(z)$, $B(z)$ and $C(z)$ are defined by the relations (48a) through (48e) with the substitution $q_z \rightarrow z$, which is used here for convenience. By solving the above

equation formally for z , we can transform it to the form $z = f(z)$, where

$$f(z) = \sqrt{\frac{-B(z) + \sqrt{B^2(z) - 4A(z)C(z)}}{2A(z)}}. \quad (61)$$

The special cases discussed in Sections 5.1 and 5.2 provide several simplifications. For example, in the case of propagation in the XZ plane and polarization along Y (s -mode), we have

$$F(z) = z^2 + k_x^2 - k^2 \eta_y(z), \quad (62a)$$

$$f(z) = \sqrt{k^2 \eta_y(z) - k_x^2}. \quad (62b)$$

Since $\eta_\alpha(z) = \eta_\alpha(-z)$, the choice of square root branch in (62) is insignificant. The same is true for the outer square root branch in the general expression for $f(z)$ (61). However, the two branches of the inner square root give rise to two different polarization modes. Thus, the simplified equation for s -polarization (62) was obtained by choosing one particular branch for the inner square root in (60); the other branch gives rise to the p -polarized mode, which is described by the equation (49c).

In the fixed-point iteration, we start from the initial guess z_0 and update it iteratively according to $z_{n+1} = f(z_n)$. We can run the iteration until it converges with required precision using the stop condition $|F(z_n)| \leq \epsilon$, where ϵ is a predetermined small constant. Alternatively, we can use fixed-point iteration to generate the initial three points for the rational approximation method. The latter requires an initial guess consisting of three values of the argument, z_1 , z_2 and z_3 , and the corresponding values of $F(z)$, F_1 , F_2 and F_3 . We then approximate $F(z)$ as

$$F(z) \cong K \frac{z - a}{z - b}.$$

From the initial guess, we find

$$a = \mathcal{N} / \mathcal{D},$$

where

$$\begin{aligned} \mathcal{N} &= F_2 F_3 z_1 (z_2 - z_3) + F_1 F_2 z_3 (z_1 - z_2) \\ &\quad + F_1 F_3 z_2 (z_3 - z_1), \\ \mathcal{D} &= F_1 F_2 (z_1 - z_2) + F_2 F_3 (z_2 - z_3) \\ &\quad + F_1 F_3 (z_3 - z_1). \end{aligned}$$

and then define the general four-point iteration

$$z_{n+1} = \frac{\mathcal{N}_{n+1}}{\mathcal{D}_{n+1}},$$

where

$$\begin{aligned} \mathcal{N}_{n+1} &= F_{n-1} F_n z_{n-2} (z_{n-1} - z_n) + F_{n-2} F_{n-1} z_n (z_{n-2} - z_{n-1}) \\ &\quad + F_{n-2} F_n z_{n-1} (z_n - z_{n-2}), \\ \mathcal{D}_{n+1} &= F_{n-2} F_{n-1} (z_{n-2} - z_{n-1}) + F_{n-1} F_n (z_{n-1} - z_n) \end{aligned}$$

$$+ F_{n-2} F_n (z_n - z_{n-2}).$$

The rational approximation iteration appears to be converging in most cases we have considered. As is well known, the convergence rate of this method is super-linear but not as fast as that of Newton's method (quadratic). We however wish to avoid the additional uncertainty of computing the derivative numerically. Therefore, we did not implement Newton's method for the simulations of this paper.

Note that application of the rational approximation method does not require generation of the initial guess by fixed-point iteration. Any three points z_1 , z_2 and z_3 can be used to this end. For example, we can take $z_1 = 0$, $z_2 = \delta$ and $z_3 = 2\delta$, where δ is a small real-valued constant. However, generation of the initial guess by fixed-point iteration is a more advantageous approach.

Another comment that should be made is that the general definition of $F(z)$ (60) does not contain square roots and therefore does not allow one to select a polarization mode by selecting a square root branch. However, equation $F(z) = 0$ has two solutions in the first Brillouin zone, not one. These solutions correspond to the different polarization modes. In contrast, equation $z = f(z)$ where a particular branch of the square root has been chosen¹⁰ has only one root in the first Brillouin zone.

Finally, we recall that the functions $f(z)$ or $F(z)$ are defined for generic z whose real part is not restricted to the first Brillouin zone of the lattice. However, if z^* is a solution to $F(z) = 0$ (in this context, the star is not related to complex conjugation), then, at least theoretically, $z^* + 2\pi n/h$ is also a solution, with n being an arbitrary integer. Let $z = x + iy$. We are seeking solutions in the first Brillouin zone, that is, satisfying

$$-\pi/h < x \leq \pi/h. \quad (63)$$

In general, a solution found numerically by one of the methods described above is not guaranteed to satisfy (63). At the frequencies above the first band gap, this is almost never the case. We therefore employ the following correction algorithm. Once a root z^* is found, we check whether it satisfies (63). If yes, no correction is needed. If no, we translate the root to the first Brillouin zone by the operation $[z^*]_{\text{FBZ}} = z^* - (2n+1)\pi/h$, where $n = \text{floor}(xh/2\pi)$. If $|n|$ is greater than some critical value (typically, 0 if strict precision is required or 1 if some small errors can be tolerated), we check whether $[z^*]_{\text{FBZ}}$ still satisfies the underlying equation by applying the condition $|F([z^*]_{\text{FBZ}})| \leq \epsilon$, where ϵ is the same small constant that was used in the main iteration. In some cases, we relax the condition by replacing ϵ with 2ϵ , which has a minor effect on precision and allows one to avoid an increase of the computation time. If however the condition does not hold, we use $[z^*]_{\text{FBZ}}$ as the initial guess for yet another search, which almost always finds the solution in the first Brillouin zone with the required precision. If this algorithm fails to find the solution with required precision,

¹⁰We can fix the branch by requiring that $0 \leq \arg(\sqrt{z}) \leq \pi$ for first branch and $\pi < \arg(\sqrt{z}) \leq 2\pi$ for the second branch.

which can occur at high frequencies, we conclude that the root searching algorithm has failed, and no dispersion point is added to the data set.